5-25-2018 9:30 AM

Glycopolymer Functionalization of Polymersomes

Josh Jadischke
The University of Western Ontario

Supervisor
Gillies, Elizabeth R.
The University of Western Ontario

Graduate Program in Chemistry
A thesis submitted in partial fulfillment of the requirements for the degree in Master of Science

Abstract

Carbohydrates are important to cellular communication, recognition, and pathogenesis, making them a useful synthetic target for application in therapeutics and diagnosis. Synthetic carbohydrate presenting scaffolds can replicate or interrupt the binding interactions that occur in nature. Due to the weak nature of the monosaccharide-protein bond, most carbohydrate presenting scaffolds display saccharides in a multivalent manner to improve binding. Recently there has been an effort to combine carbohydrate containing scaffolds with polymersomes (vesicles composed of polymers), due to the structural resemblance of polymersome membranes to biological membranes. This thesis describes the progress towards functionalizing polymersomes with linear glycopolymers as a potential method to achieve improved multivalent binding. A novel β-D-Galactose containing polymer was synthesized using reversible addition-fragmentation chain transfer polymerization. This polymer, as well as a previously reported glycopolymer based on a polyacrylamide backbone were labeled with rhodamine in order to quantify their subsequent conjugation to the polymersome surface. Two different vesicle platforms were investigated, polybutadiene-b-poly(ethylene glycol) and poly(ethylene glycol)-b-poly(ethyl glyoxylate)-b-poly(ethylene glycol). The experiments suggested that it is possible to conjugate the glycopolymers to the polymersome surfaces to obtain different glycopolymer densities and quantify the reaction yields using fluorescence spectroscopy. Future work will involve binding studies of the glycopolymer-coated vesicles to carbohydrate binding proteins (lectins).

Keywords

Carbohydrates, glycopolymers, carbohydrate scaffolds, polymersomes, vesicles, surface functionalization, RAFT, multivalency.

Co-Authorship Statement

The work presented in this thesis is the result of the author's work as well as the work of coworkers at Western University and Dr. Elizabeth Gillies whose exact contributions are described here.

Chapter 1 was written by the author and edited by Dr. Elizabeth Gillies

Chapter 2 describes an ongoing project proposed by Dr. Elizabeth Gillies. Both **PAGal** glycopolymers were synthesized and characterized by Brooke Raycraft. Synthesis and characterization of the **PEtG$_{UV}$** was performed by Dr. Bo Fan and Dr. Kai Cao. Dr. Fan also synthesized and characterized the **MeO-PEtG$_{Thermo}$-PEG-OMe**. All other work was performed by the author.

Chapter 3 was written by the author and edited by Dr. Elizabeth Gillies.

Chapter 4 was written by the author and edited by Dr. Elizabeth Gillies.

Acknowledgments

I would like to first and foremost thank Dr. Gillies for being my supervisor. She taught me so much. From crucial soft skills, like effective and clear communication, to technical skills, like comprehensive NMR analysis. I will be forever grateful for the numerous learning opportunities she gave me. Finally, I cannot thank her enough for all the times she went above and beyond to edit reports for me.

My thanks go out to everyone I have had the pleasure working with in the Gillies Group. Thank you for your words of wisdom on chemistry and unrelated topics. I am grateful to have had the opportunity to get know some of you very well and look forward to the long years of friendship to come. I wish the best for every one of you.

I would to say a heartfelt thank you to my parents who have supported me along my academic journey. It would have been impossible to have reached this point in my life without your guidance. To my sister, thank you for always being there.

Finally, I must thank my girlfriend Meghan for her advice, continuous support, and words of encouragement. I greatly appreciate the different perspective you always have to offer. Thank you for helping me through the late nights of writing reports, and for being more than willing to read them.

Table of Contents

List of Tables

List of Figures

List of Schemes

List of Abbreviations

AIBN	Azobisisobutyronitrile
ATR	Attenuated Total Reflectance
BHT	Butylated hydroxytoluene
BPS	Bathophenanthrolinedisulfonic acid disodium salt hydrate
CLSM	Confocal Laser Scanning Microscopy
CTA	Chain Transfer Agent
CuAAC	Copper Azide-Alkyne Cycloaddition
$Đ$	Dispersity
DCC	*N,N'*-Dicyclohexylcarbodiimide
DIPEA	*N,N*-Diisopropylethylamine
DLS	Dynamic Light Scattering
DMAP	4-Dimethylaminopyridine
DMF	Dimethylformamide
DMSO	Dimethyl sulfoxide
DP_n	Degree of Polymerization
DPTS	4-(Dimethylamino)pyridinium 4-toluenesulfonate
DSC	Differential Scanning Calorimetry
ECM	Extracellular Matrix
EDC·HCl	*N*-(3-dimethylaminopropyl)-*N'*-ethylcarbodiimide hydrochloride

FT-IR	Fourier-transform infrared spectroscopy
GNP	Gold Nanoparticle
iNKT	invariant Natural Killer T
MBP	Mannose Binding Protein
M_n	Number Average Molar Mass
MWCO	Molecular Weight Cut Off
NMR	Nuclear Magnetic Resonance
PBD	Polybutadiene
PEG	Poly(ethylene glycol)
PEtG	Poly(ethyl glyoxylate)
RAFT	Reversible Addition-Fragmentation Chain-Transfer
SABP	Sialic Acid Binding Proteins
SEC	Size Exclusion Chromatography
TEG	Tri(ethylene glycol)
T_g	Glass Transition Temperature
TEM	Transmission Electron Microscopy
TGA	Thermogravimetric Analysis
THF	Tetrahydrofuran
TLC	Thin Layer Chromatography
T_o	Onset of Decomposition Temperature

Chapter 1

1 Carbohydrates and their Role in Therapeutics

1.1 Introduction to Carbohydrates

1.1.1 Carbohydrates and their role in Nature

Carbohydrates or saccharides play a crucial role in cellular adhesion and molecular signaling that occurs at the surfaces of many mammalian and microbial cells.[1,2] The interactions between cells and the surrounding extracellular matrix (ECM) are regulated by cellular adhesion events that fall under one of three interaction types: protein-protein, protein–carbohydrate, and carbohydrate–carbohydrate interactions. These interactions control the binding of connective proteins that form the ECM.[3] Carbohydrates displayed on the surfaces of cells act as identifying molecules that inform cells of their respective type, thereby allowing for cellular organization and the formation of homogeneous-multicellular tissue.[4,5] Signaling molecules regulate the immune response, cancer metastasis, and act as indicators for disease states in the human body.[5]

1.1.2 Carbohydrates and the Human Immune System

The innate and adaptive immune systems mimic key interactions between displayed carbohydrates and complimentary binding proteins on the surface of mammalian cells and pathogens in order to fight infection. The innate immune system is the part of the immune system that can protect the body from a wide variety of pathogens. It is partially composed of different types of phagocytes that can consume and destroy pathogens. For example, macrophages can identify and trap a virion by multiple carbohydrate-based mechanisms.[5] Mannose Binding Proteins (MBPs) found in the blood stream can bind to mannose residues displayed on the surface of a virion to form a complex.[6] MBP-virion

complexes can then associate with receptors on the surface of the macrophage to trigger phagocytosis (Figure 1.1).[5,7] Phagocytosis can also be triggered by the binding of sialic acid residues displayed on a macrophage's surface sialic acid binding proteins (SABP) or long linear pendent protein chains to virion surface proteins[8]; sialic acid functionalized protein chains act like a net in the blood stream, attempting to capture pathogens that do not make direct contact with the macrophage's surface.[5]

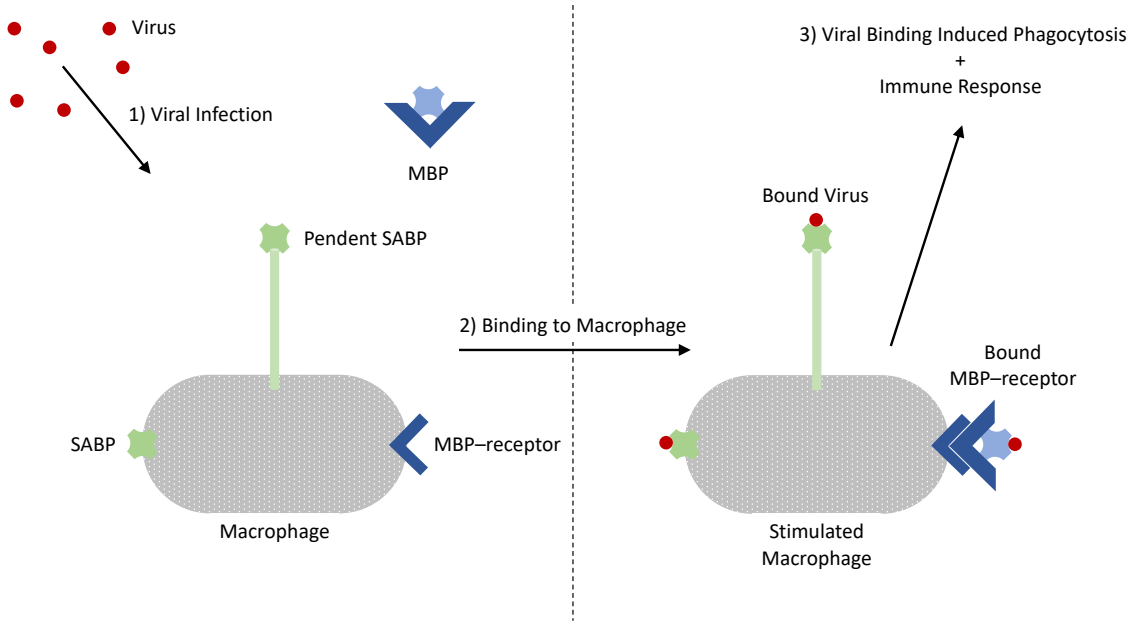

Figure 1.1. Binding of viruses to a macrophage presenting MBP-Receptors and SABP's to induce phagocytosis and an immune response.

Although the innate immune system provides defense against many invading pathogens, the adaptive immune system allows for a long term and larger immune response than the innate system. Dendritic cells, a type of phagocyte from the innate immune system, display fragments of glycoproteins or glycolipid complexes that were derived from a previously consumed virion. Specialized lymphocytes interact with the presented fragments and use the information to trigger an immune response. A dissimilar immune response targeting the human body's own cells can be triggered by abnormal or pathogenic carbohydrate displays on the surface of human cells.

1.1.3 Carbohydrates and Cancer

The body can identify cancerous cells by the aberrant presentation of carbohydrates on the surface of the cell.[9] Malignant cancer cells often have different carbohydrates presented due to the fact that they have different cellular adhesion and mobility than typical cells.[10] Increased glycosylation of surface glycoproteins has been observed in multiple types of cancer including breast, prostate, and pancreatic cancers.[10] Higher degrees of glycosylation have been speculated to increase the ability of tumors to metastasize by improving binding of the cancerous cells to the walls of blood vessels.[10] Unique and cancer specific antigens are displayed by cancerous cells.[11] Thus, these antigens have been considered to be a useful target for potential cancer vaccines or targeted drug delivery. Carbohydrates have widely been hailed as potential therapeutics but to understand the design of such therapeutics, a closer look at the nature of carbohydrate bonds is required.

1.2 The Nature of Carbohydrate Binding

1.2.1 Carbohydrate–Protein Binding

Carbohydrates typically bind to proteins and other carbohydrates through weak intermolecular forces. When binding to proteins, carbohydrates typically bind either in pockets or grooves on the surface of a protein. Pockets only allow specific saccharides with a certain conformation to favourably bind (Figure 1.2); grooves offer a less specific binding. Non–covalent hydrogen bonding of saccharide hydroxyl groups to aspartic acid, asparagine, glutamic acid, glutamine, and arginine residues are the most important and strongest binding interactions.[12,13] The formation of new hydrogen bonds is important to the spontaneous binding of saccharide to proteins. However, to understand the binding of mono-, oligo- or polysaccharides to proteins, driving forces other than hydrogen bond formation must also be introduced.[13]

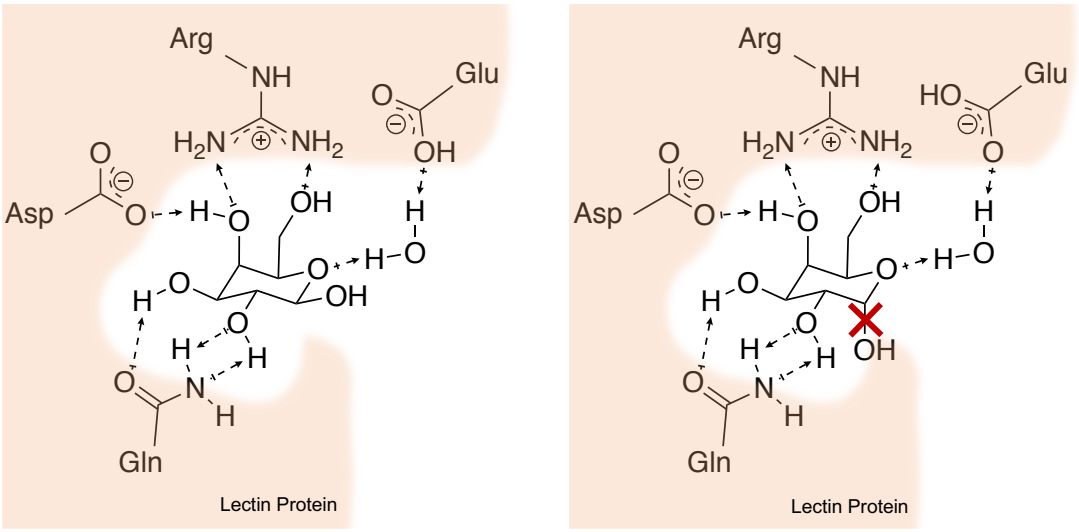

Figure 1.2. Schematic illustrating the effect of binding of galactose to a binding pocket. *β*-galactose favourably binds to the protein where α-galactose does not bind favourably due to steric hindrance.[12]

The spontaneous binding of carbohydrate presenting molecules to complimentary lectins is assumed to be a model system for carbohydrate-protein binding interactions. "Lectins are proteins of nonimmune origin that bind to specific carbohydrates without modifying them," and have been found in most microorganisms and multi-cellular organisms.[5,13] In a binding interaction, initially both the carbohydrate and site of binding are solvated, typically with water molecules. The water molecules at the site of binding are suspected to be highly ordered and in a higher-energy state than water molecules interacting in bulk.[13] When the carbohydrate hydroxyl groups interact with amino acid residues at the site of binding, the high-energy water molecules are displaced, and become lower in energy.[13,14] The breaking of the hydrogen bonds contributes a small negative ΔH term to ΔG, in $\Delta G = \Delta H - T\Delta S$, where a negative ΔG indicates spontaneous binding. There is an enthalpic cost associated with the formation of new water–water hydrogen bonds, but it is

compensated for by the slightly larger entropic contribution of solvent rearrangement to ΔS.[15] The rearrangement of highly–ordered water molecules surrounding the hydrophobic portions of the carbohydrate and lectin binding site to disordered water molecules is highly favours entropy. Thus, solvent rearrangement is the main driving force behind carbohydrate–lectin binding.[13,15] The binding site favours the binding of a specific conformation of the carbohydrate, but conformational binding and locking reduces the rotational freedom of the carbohydrate bonds. This reduction in rotational freedom is associated with a small entropic cost that makes ΔG slightly less negative. Monosaccharide-lectin binding is determined by the above enthalpic and entropic interactions.[4] Oligosaccharides and molecules that present multiple copies of a saccharide have a more favourable binding to lectins due to the multivalent effect.

1.2.2 Multivalent Carbohydrate Binding to Lectins

The increased binding of oligosaccharides, glycopolymers, glycoproteins, and glycolipids in biological systems may offer an explanation for why many key binding interactions rely on molecules displaying multiple carbohydrates. One reason multivalent carbohydrate binding moieties may have stronger interactions with lectins, is that lectins and some other proteins contain multiple binding sites.[13] For example, in the binding of glycopolymers, an entropic cost is initially paid when one of the saccharides adapts the required binding conformation; flexible and freely rotating glycopolymers have more entropy than bound glycopolymers.[13] Other saccharides on the glycopolymer are now free to bind to another site on the lectin without paying the same initial entropic cost, increasing the favourability of the second saccharide binding event. Upon binding of a multivalent carbohydrate there may also be a large local concentration of saccharides, contributing to the multivalent effect. After a single saccharide binds to the complementary lectin, many saccharides populate the local environment, shifting the equilibrium to favour binding. It can be imagined that either interactions with another binding site, or interaction with the same binding site, after disassociation, would be possible.[5,13] The multivalent effect on binding is expected to be driven by a combination of entropic and concentration–based effects.[4] Due to the increased binding and

prevalence of polyvalent carbohydrates in nature, many therapeutic scaffolds taking advantage of the multivalent effect have been proposed over the years.

1.3 Carbohydrate Presenting Scaffolds for use in Therapeutics

1.3.1 Naturally Occurring Glycopolymers

Scaffolds presenting polyvalent carbohydrates are often designed to replicate carbohydrate presentation in nature. A natural glycopolymer that has been shown to have many therapeutic applications is hyaluronan, a derivative of hyaluronic acid (Figure 1.3). Hyaluronan is a glycopolymer found in many living organisms and in the ECM of cartilage in humans.[16] It has applications in ophthalmology, treatment of osteoarthritis, and wound healing, where the hyaluronan often acts as a lubricant or moisturizer.[17] Hyaluronan can be modified through semi-synthetic methods to alter the properties. However, synthetic glycopolymers offer distinct advantages over natural or semi-synthetic glycopolymers.

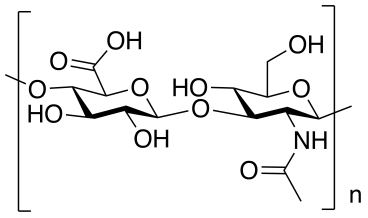

Hyaluronic Acid

Figure 1.3. Structure of Hyaluronic Acid, a natural glycopolymer.

1.3.2 Synthetic Glycopolymers

Synthetic glycopolymer scaffolds have been developed to control structural properties including molar mass and the presented saccharide. A high degree of variability in molar mass (number of presented saccharides) within a particular glycopolymer sample, or a polydisperse sample, increases the variability of action for biological applications. In contrast, monodisperse samples, or samples with a low degree of variability in molar mass, have reproducible properties and less therapeutic variability.[5,18] Glycopolymers with a molar mass under 100,000 g/mol have been shown to avoid stimulating parts of the immune system, creating greater specificity of action.[10] The carbohydrate presented often determines the application of a glycopolymer. For example, the Influenza A virus is coated in proteins that specifically bind to sialic acid.[5,19,20] A natural glycopolymer containing sialic acid residues, mucin, can neutralize a virus as seen in Figure 1.4 (a). Tsuchida and co-workers took advantage of this and designed a synthetic glycopolymer with sialic acid residues to neutralize the infectious capability of viral particles as shown in Figure 1.4.[20] Short synthetic glycoproteins, or glycosylated polypeptide sequences, have been shown to have similar neutralization potential to viral particles.[21]

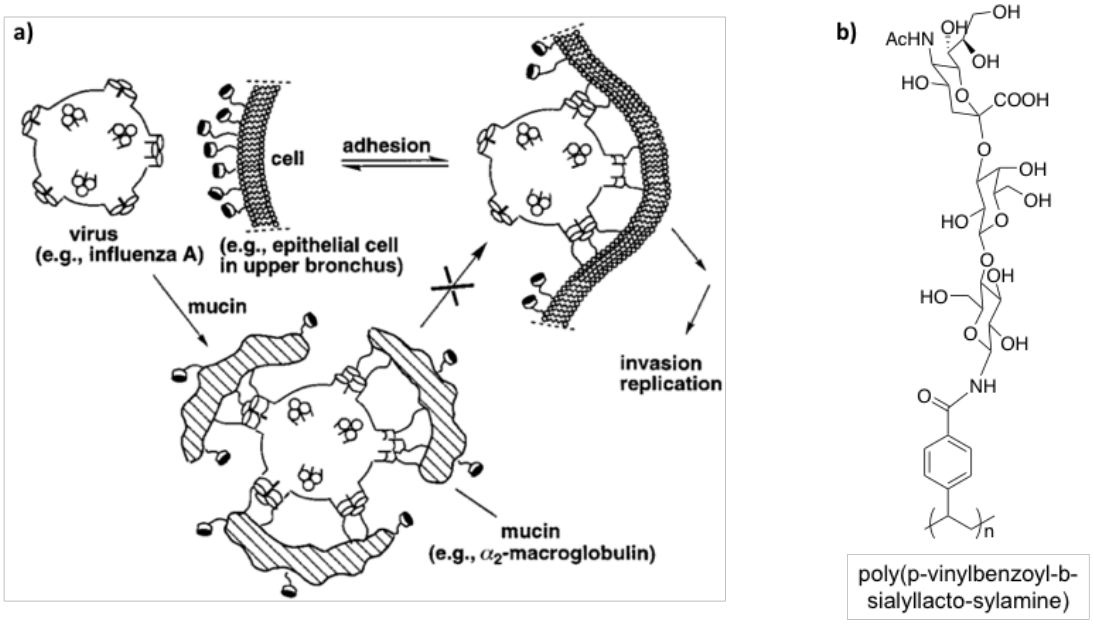

Figure 1.4. (a) Neutralization of an influenza virus with mucin, a natural glycoprotein containing sialic acid groups. The mucin inhibits binding of the virus to the cell,

preventing invasion. Modified and reprinted with permission.[19] (b) Structure of sialic acid glycopolymer derivative used to neutralize Influenza A.

1.3.3 Glycopeptides

Glycopeptides are synthetic glycopolymers based on peptide linkages between glycosylated amino acid derivatives. Peptide synthesis involves sequential deprotection and protection steps leading to discrete peptide sequences which improves the reproducibility of experimental results.[22] Control over the peptide sequencing allows for the fine tuning of distances between binding groups and can change the presented carbohydrate patterns.[23] For example cyclic glycopeptides present carbohydrates in a unique manner (Figure 1.5).[21] Synthetic glycoproteins, as a class of scaffolds, are generally highly biocompatible due to the fact that most organisms possess the enzymes to break down peptide linkages.

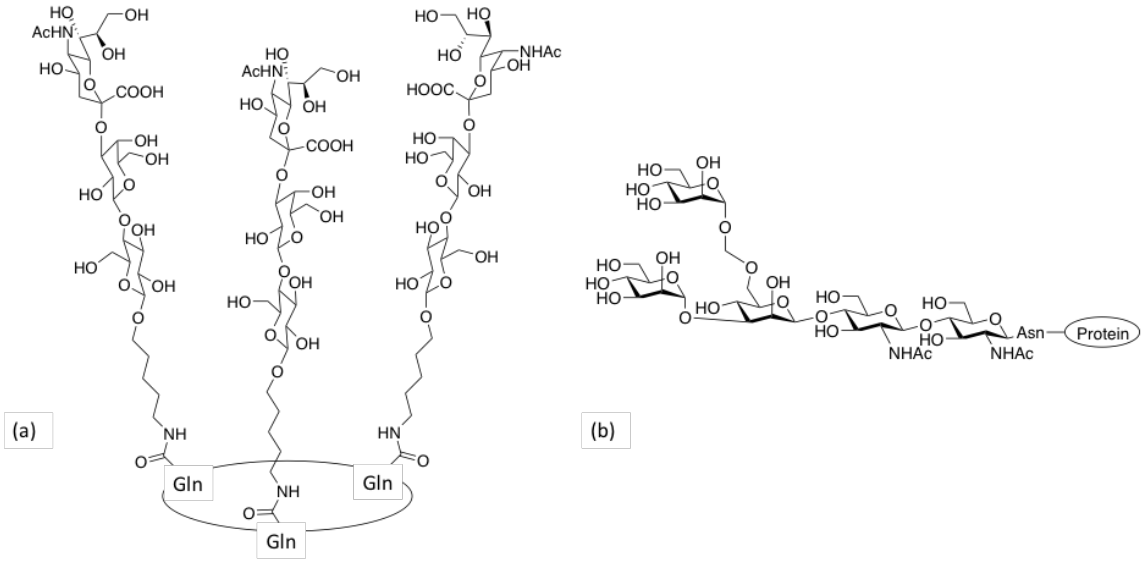

Figure 1.5. (a) Sialylated lactose cyclic glycopeptide shown to neutralize Influenza A.[21] (b) Pentasaccharide core of N-glycans.[24]

1.3.4 Glycoconjugates

Glycoconjugates are another biocompatible scaffold that use glycosylated proteins, antibodies, or antigens as therapeutics. The term glycoconjugate refers to any protein or antibody that has a glycopolymer, oligosaccharide, or glycopeptide covalently bound, or conjugated, to its surface to improve its targeted delivery.[5] *N*-glycans are an example of naturally occurring glycoconjugates. *N*-Glycans have the same pentasaccharide core as shown in figure 1.5 with functionalization of the hydroxyls observed.[24] Although glycoconjugates show potential for a wide variety of applications, available synthetic transformations are limited to reaction conditions that will not destroy the biological activity of the protein.[24,25] Glycosylation reactions often require anhydrous conditions which are incompatible with many proteins.[23] The present synthesis of glycoconjugates, like *N*-glycans, relies on enzymatic transformations which have issues of site-specific reactivity.[24,25] Despite difficulties with synthesis, glycoconjugate therapeutics have been developed. For example, branched glycoproteins conjugated to a protease that could cleave a specific receptor on a bacterial pathogen. The glycoconjugate of the protease showed an improvement in efficacy by 10^3 over the protease.[5]

1.3.5 Glycodendrimers

Glycodendrimers are a class of branched glycopolymers that are both well-defined and present carbohydrates in a multivalent manner.[26] The molecule typically branches away from a central point with selected reactive or functional groups at the outer terminus.[26] Dendrimers are often synthesized generationally using a series of protection, coupling, and deprotection steps similar to polypeptides.[7,27] Each growth step increases the generation and branching of dendrimers, where G0 is the initial generation and the third generation, G3, has had at least three growth steps increasing the branching. These discrete generational synthetic steps lead to high degrees of control over the size and consequently the size dependent properties. The effect of dendrimer generation and number of presented saccharide units was observed in a study by André *et al.* where they tested lactose functionalized glycodendrimers as an inhibitor of $(AB)_2$-toxic agglutinin, a

toxic lectin found in mistletoe.[28] Glycodendrimers of generation G3-G5, displayed 32 (Figure 1.6) to 128 lactose molecules, which showed a 10 to 100 fold increase in relative inhibition potency over lower generation dendrimers, G0-G2, which displayed 4 to 16 lactose molecules.[28] A high-density of terminal functional groups increases binding affinity for certain systems. [18]

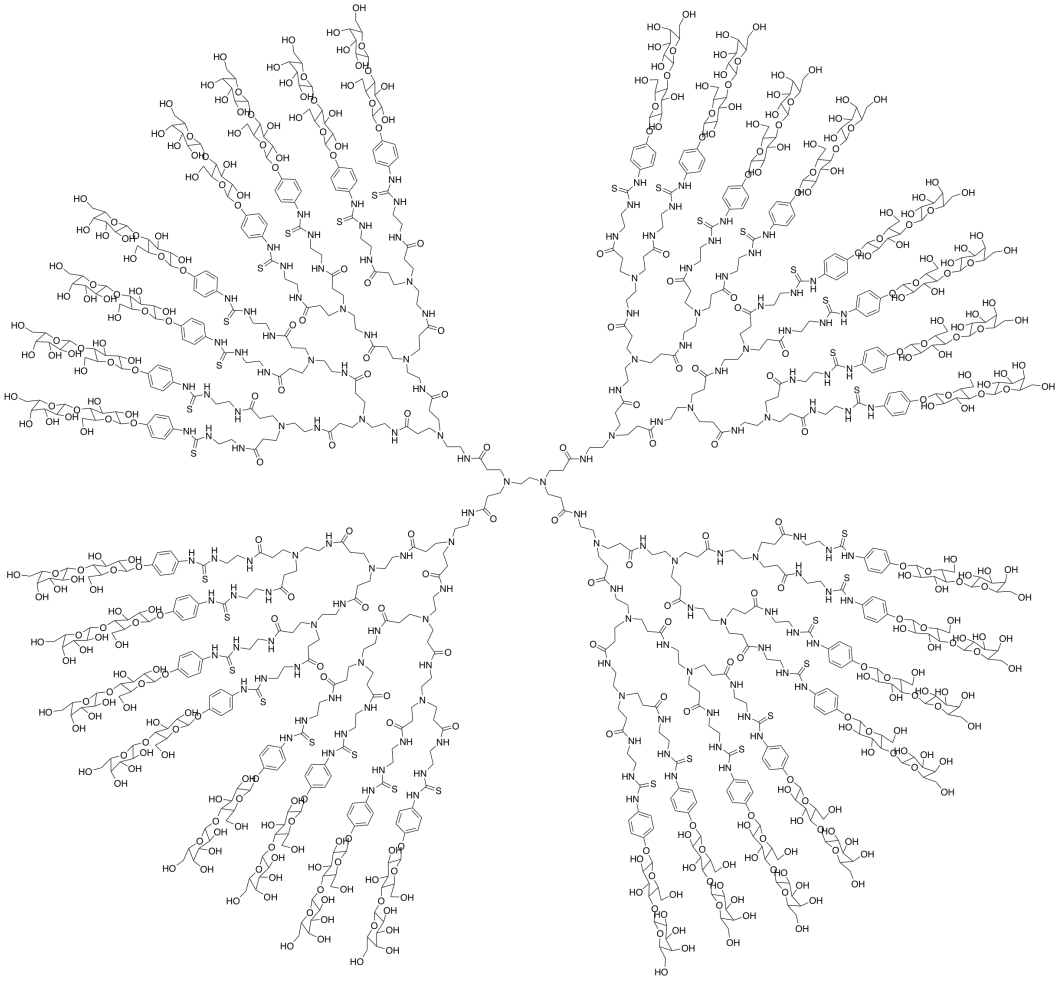

Figure 1.6. Structure of the lactose–functionalized starburst glycodendrimer synthesized by André *et al*.[28]

1.3.6 Carbohydrate Functionalized Nanoparticles

Functionalized nanoparticles composed of gold, iron oxide, and other semi-conductive metal nuclei have been functionalized with carbohydrates creating the field of glyconanoparticles.[29] The metallic nucleus of a glyconanoparticle gives the particle inherent magnetic and electrochemical properties, and the use of a radionuclide makes a glyconanoparticle a multimodal imaging scaffold.[29] Goldnanoparticles (GNP) functionalized with lactose, Figure 1.7, showed strong binding to galectin-1, a mammalian β-galactoside-specific lectin.[30] An overcrowding effect was observed with the lacto-GNP, where a decreased binding to the lectin was associated with 100 percent surface functionalization.[30] Similar lacto-GNP were applied in anti-adhesion therapy in mice.[31,32] The metastasis of a melanoma cell line in mice treated with lacto-GNP was inhibited up to 70% in comparison to untreated mice.[32] Cationic glycopolymer functionalized GNPs have shown potential as gene delivery vehicles. The particles had a transfection efficiency of approximately 55 %.[33]

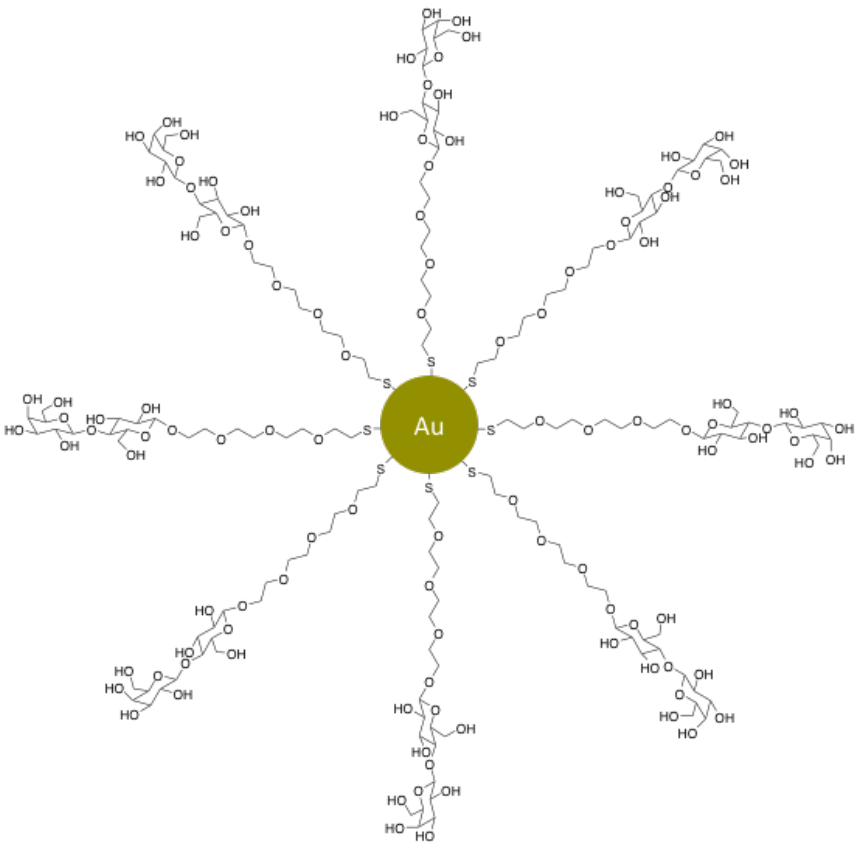

Figure 1.7. Simplified representation of a lactose–functionalized goldnanoparticle.[30]

1.4 Carbohydrate Presenting Assemblies and their Applications

1.4.1 Micelles

Nano-assemblies composed of amphiphilic molecules have been of interest to scientists for many years due to their abilities to encapsulate a variety of hydrophilic and hydrophobic cargo and their ability to mimic cell membranes.[34] Amphiphilic molecules can spontaneously self-assemble to form unique morphologies, usually determined by the hydrophilic weight fraction of the molecule.[34] Micellar morphologies have been observed from the self-assembly of amphiphilic glycopolymers. For example, Suriano *et al.* synthesized a galactose–functionalized polycarbonate block copolymer using ring

opening polymerization (Figure 1.8 (a)). From the block copolymer they were able to form micelles that could be loaded with doxorubicin, an anti-cancer drug. The galactose-functionalized micelles showed specific uptake into liver carcinoma cells (HepG2) over glucose functionalized analogues. The results therefore indicated the potential for targeted delivery of anti-cancer drugs using glyco-assemblies.[35] The micellar morphology allows for the loading of hydrophobic cargo, however hydrophilic cargo may be loaded into a variety of other assembly morphologies.

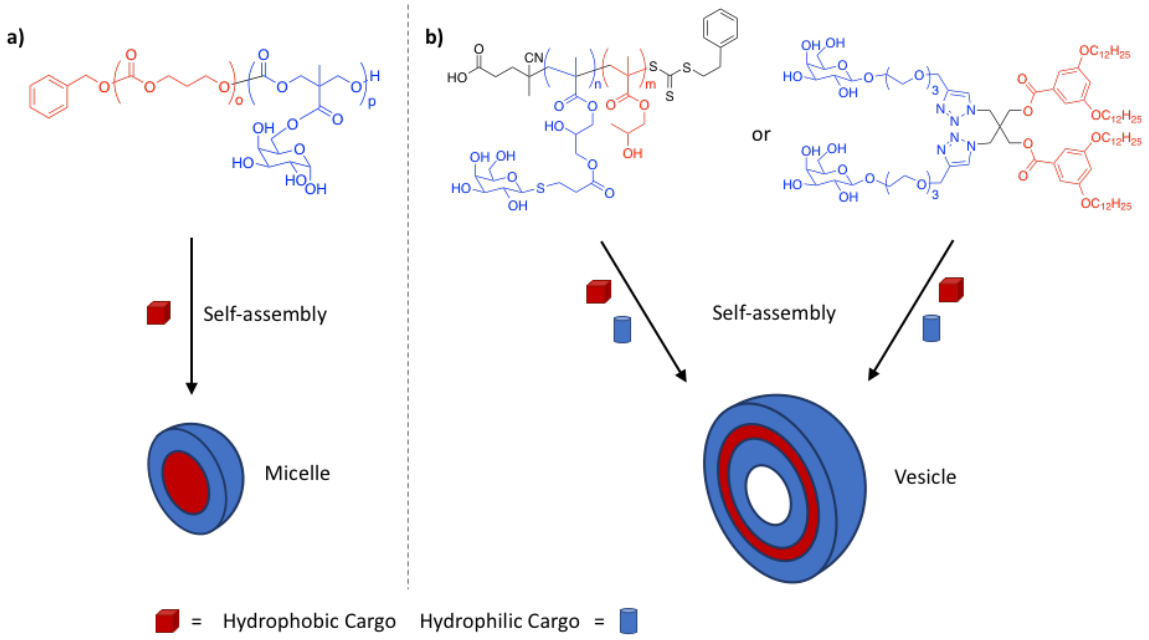

Figure 1.8. (a) Self–assembly of galactose-functionalized amphiphilic polycarbonate-based polymer into a micelle loaded with hydrophobic cargo.[35] (b) Self–assembly of PGalSMA amphiphilic block copolymer or a twin-twin amphiphilic glycodendrimer into a vesicle loaded with hydrophobic and hydrophilic cargo.[36,37]

1.4.2 Polymersomes

A vesicle morphology is observed when a bi-layer is formed during the self-assembly of amphiphilic molecules. Vesicles have been observed to result from the self-assembly of lipids, dendrimers, and block copolymers.[38,39] Polymethacrylate block copolymers

conjugated with galactose (PGalSMA) have been synthesized using reversible addition–fragmentation chain–transfer (RAFT) polymerization. RAFT is a method of controlled polymerization that can afford monodisperse polymer samples, or samples that contain polymer chains all of similar molecular weight.[40] Monodisperse polymer samples are important for self–assembly due to the sensitive nature of the hydrophilic–hydrophobic ratio that determines assembly morphology. It is common for amphiphilic block copolymers used in therapeutic scaffolds, PGalSMA for example, to be synthesized using RAFT polymerization to improve reproducibility and reliability.[41] PGalSMA has been shown to assemble into vesicles (Figure 1.8 (b)).[36] A hydrophilic rhodamine-based dye that cannot normally undergo cellular uptake was loaded into the PGalSMA vesicles. Staining of internal cellular organelles indicated cellular uptake and successful cargo delivery. [36]

1.4.3 Dendrimersomes

Percec and coworkers have synthesized Janus glycodendrimers using a modular strategy that allowed the authors to produce vast libraries of glycodendrimers.[38] The libraries enabled them to determine the effects of crystallinity, saccharide, and linker lengths on assembly morphology.[37] Glycodendrimers with a variety of saccharides were able to form giant glycodendrimersomes, which are assemblies of micrometer-scale. Due to their size, bi-layer membrane, and multivalent presentation of surface carbohydrates, the glycodendrimersomes were presented as a new potential cellular mimic.[38] Gillies and co-workers synthesized α-galactose-presenting glycodendrimers which could self–assemble into vesicles. These α-galactose glycodendrimersomes were able to stimulate invariant natural killer T (iNKT) cells.[27] iNKT cells are normally stimulated by α-galactose presented in a multivalent manner, which is associated with pathogenesis.[27] Self-assemblies displaying carbohydrates in a multivalent manner provide a unique opportunity to act as delivery agents and biological mimics for use in therapeutics and the study of biological activity.

1.5 Thesis Objectives

1.5.1 Project Background

In previous work by the Gillies group, polymersomes were functionalized with dendrimers using a copper–catalyzed azide–alkyne cycloaddition (CuAAC) reaction.[39,42,43] It was determined that post-assembly modification of polymersomes using CuAAC did not disrupt the assembly morphology.[42] Varying degrees of surface functionalization were possible by altering the ratio of azide-functionalized to unfunctionalized amphiphilic polymer used to form the polymersomes.[39,42,43] The Gillies group successfully functionalized polybutadiene-*b*-poly(ethylene oxide) (PBD-*b*-PEO) polymersomes with sialic acid derivatized glycodendrimers.[7] These glycodendrimer functionalized assemblies were shown to bind well to complimentary lectin but the ability of the assemblies to prevent the binding of influenza A viruses to mammalian cells was found to be limited. This was believed to result from the rigidity of the glycodendrimer structures. It can be imagined, that when surrounding a spherical virus with other spheres, the area of contact would be relatively limited. Because of the previous results, it was speculated that an improvement in binding could be achieved by introducing flexible linear glycopolymers to the surfaces of the polymersomes. This would instead allow octopus-like structures to surround the virus. Given the role of carbohydrates in numerous biological processes, it was proposed that glycopolymer-functionalized polymersomes could potentially serve as multivalent inhibitors of viral infection, vaccines, or targeted drug delivery vehicles that would resemble cell membranes. In addition, they could simultaneously serve as carriers for hydrophobic and hydrophilic cargo such as drugs or imaging agents. The surface functionalization density and glycopolymer chain length may also give important information about the optimal surface structure for lectin binding.

In unpublished Gillies group work, the successful polymerization of an acrylamide functionalized *β*-galactose monomer using RAFT had been achieved.[44] Small quantities

of alkyne terminated low molecular weight polymer, high molecular weight polymer, and monomer were previously synthesized and available for test reactions. The alkyne end-group of the polymer could potentially undergo a CuAAC reaction with azide functionalized PBD-*b*-PEG polymersomes (Figure 1.9). PBD-*b*-PEG was chosen as the amphiphilic block co-polymer because it has previously been used to produced vesicles using the film-hydration method.[42] Film hydration was selected as a method of self-assembly because it allows for the facile encapsulation of both hydrophobic and hydrophilic cargo, while generally avoiding bio-incompatible organic solvents. Preliminary experiments had been performed to investigate the coupling of the linear polymers onto the vesicles.

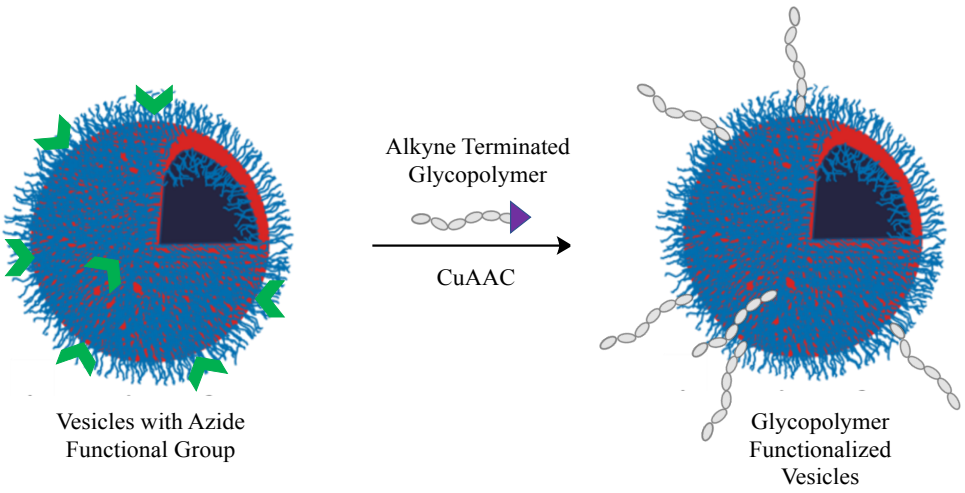

Figure 1.9. Schematic showing the method for functionalizing polymersomes with glycopolymers.

1.5.2 Project Objectives

For this thesis, it was proposed to prepare and study four different functionalized polymersome systems to examine the effects of both glycopolymer chain length and density on binding to lectin. Low and high densities of short and long polymers were

proposed (Figure 1.10). Efficacy of the CuAAC reaction between the polymersomes and glycopolymers needed to be quantified to make accurate conclusions about the effect of glycopolymer density on binding.[39,42,43] It was proposed that this could be accomplished using a similar method as shown in Figure 1.9 above, but with dye-labeled glycopolymers. This thesis describes the progress towards these goals.

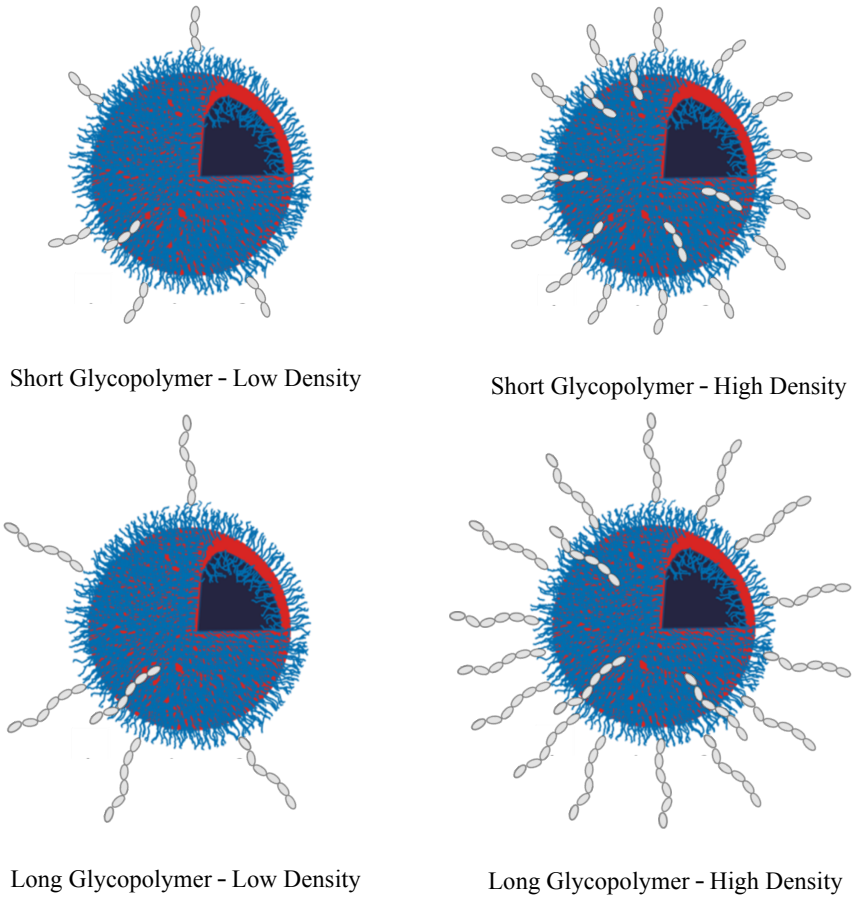

Figure 1.10. Diagram showing the four degrees of glycopolymer functionalization targeted.

Chapter 2

2 Results and Discussion

2.1 Synthesis and Characterization of Glycopolymers

In prior work by the Gillies group, polyacrylamides with terminal alkynes and pendant galactose moieties had been synthesized with two different degrees of polymerization (DP_n) and consequently two different number average molar masses (M_n). A RAFT polymerization approach had been used to provide glycopolymers with low dispersities ($Đ$). 200 mg of **PAGal$_9$** (DP_n ~9, M_n = 2,400 g/mol, $Đ$ = 1.2, based on size exclusion chromatography (SEC) in water) and 100 mg of **PAGal$_{19}$** (DP_n ~19, M_n = 5,200 g/mol, $Đ$ = 1.3) were available for test reactions on polymer vesicle surfaces.[44] To quantify the extent of reaction with the vesicle surface, a fluorescent dye was conjugated to each of **PAGal$_9$** and **PAGal$_{19}$** (Scheme 2.1). This was accomplished using a *N*-(3-dimethylaminopropyl)-*N'*-ethylcarbodiimide hydrochloride (EDC·HCl) coupling reaction in the presence of 4-dimethylaminopyridine (DMAP) to react the carboxylic acid group of rhodamine B with a small number of the hydroxyl groups of the pendant β-galactose moieties. It was desirable to modify only a small fraction of the sugars to minimize the structural modification of the polymer and therefore reduce any impact of the dye molecules on the properties of the conjugated glycopolymers. The product was purified by dialysis against water using a 1,000 g/mol molecular weight cut-off (MWCO) membrane.

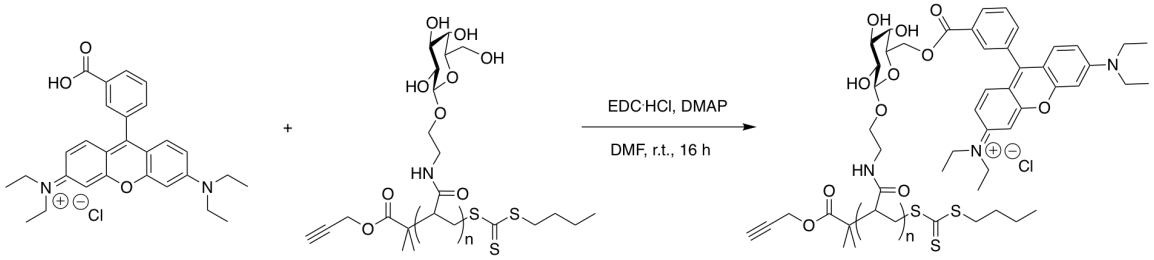

Rhodamine B | **PAGal$_9$** (n = 9) **PAGal$_{19}$** (n = 19) | **PAGal$_9$-Rho** **PAGal$_{19}$-Rho**

Scheme 2.1. Synthetic scheme for the coupling of rhodamine B onto **PAGal**.

The ^{1}H NMR spectra of the rhodamine functionalized polymers **PAGal$_9$-Rho** and **PAGal$_{19}$-Rho** had a new broad peak in the aromatic proton region that were characteristic of the rhodamine dye, indicating the successful coupling of rhodamine onto the polymer (Figure 2.1). Based on the relative integrations of peaks at ~7.5 ppm and ~4.3 ppm in the ^{1}H NMR spectra, the rhodamine was conjugated in ~7% molar equivalents for **PAGal$_9$-Rho** and ~9% molar equivalents for **PAGal$_{19}$-Rho**, compared to the individual repeat units.

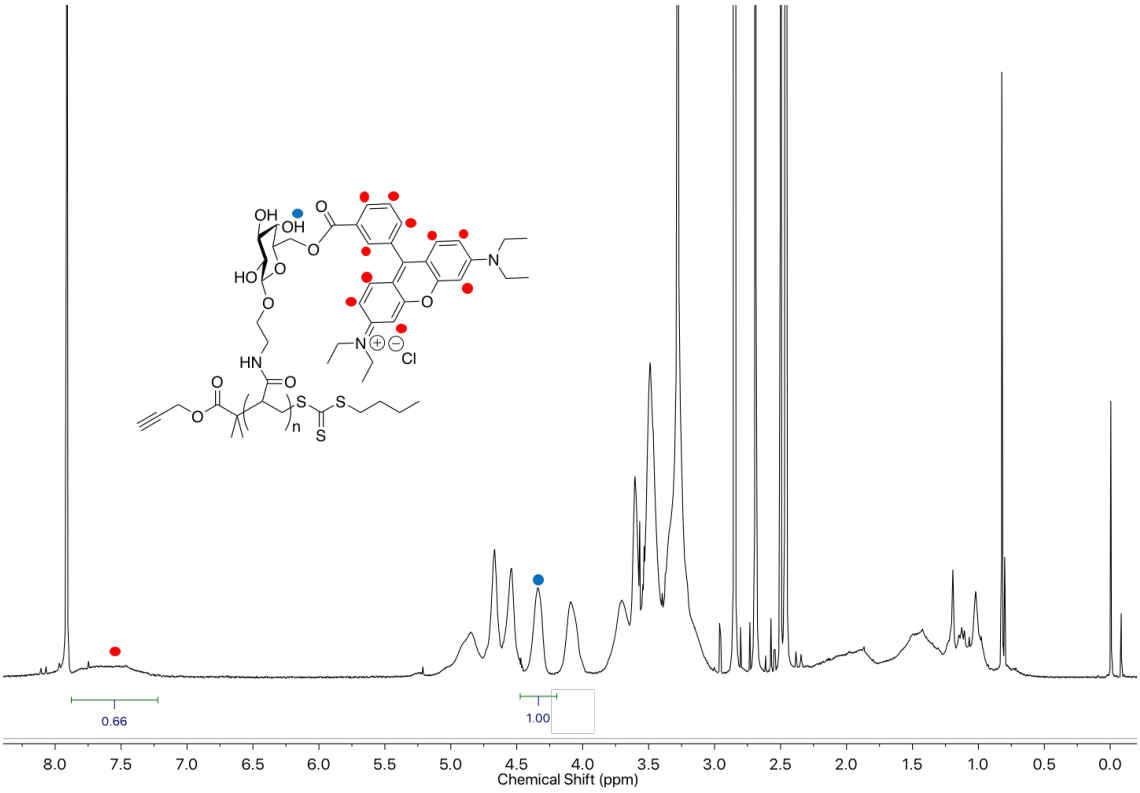

Figure 2.1. ^{1}H NMR spectra of **PAGal$_9$-Rho** showing the characteristic rhodamine dye peak (600 MHz, DMSO-d6).

Polymers **PAGal$_9$** and **PAGal$_{19}$** were suitable for test quantification reactions but for the lectin binding tests more of these polymers were required. Consequently, more of monomer needed to be synthesized and polymerized. To accomplish this, replication of the synthesis shown in Scheme 2.2 was attempted.[44] First, the pentaacetate-protected D-galactose was synthesized by the reaction of D-galactose refluxing acetic anhydride in the presence of sodium acetate. The D-galactose pentaacetate was then selectively glycosylated with azido ethanol using boron trifluoride etherate to afford the β-anomer of compound **1**. A saccharide-based impurity, < 10% by H NMR, suspected to be D-galactose pentaacetate, was observed in a ^{1}H NMR spectrum of 'purified' compound **1**. After multiple attempts to purify compound **1** further using column chromatography, the synthesis was continued with the hope that purification at a later step would be possible.

The azide group in compound **1** was reduced using Lindlar's catalyst, Pt on $CaCO_3$ poisoned with 5% Pb, suspended in ethanol in a hydrogen gas environment. To avoid a reaction of the newly formed amine group and the acetyl protecting group, para-toluene sulphonic acid was used as a temporary protecting group by forming the ammonium salt, compound **2**. In the final step, to afford monomer **AAcGal**, the ammonium group was deprotonated with excess *N,N*-diisopropylethylamine (DIPEA) allowing for the formation of the amide with the acryloyl chloride.

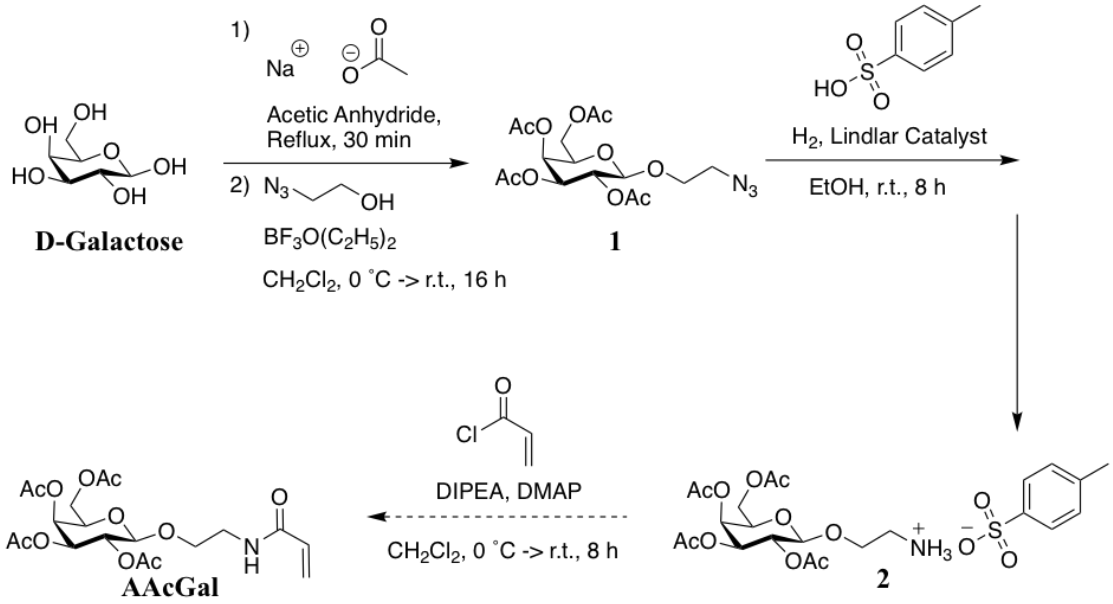

Scheme 2.2. Synthesis of monomer **AAcGal**, *β*-D-galactose pentaacetate functionalized acrylamide monomer.

A high degree of difficulty with the synthesis and purification at the final step of synthesizing monomer **AAcGal** was experienced. The TLC of crude **AAcGal** showed multiple products with 3 spots staining with ninhydrin, indicating the presence of an amine or amide. After collecting what seemed to be the product containing fractions from column chromatography, the ^{1}H NMR spectrum still indicated the presence of impurities which were not removed upon re-purification with column chromatography. It should be

noted that after the first column, the yield dropped from ~14 g of crude product to ~ 4 g. It had been previously reported in unpublished Gillies group work that this acrylamide monomer was exceptionally reactive and could auto polymerize. Butylate hydroxytoluene (BHT), a radical inhibitor, was added to the eluent to prevent auto-polymerization, but the drastic decrease in yield could still be attributed to auto-polymerization of the monomer on the column and removal of the impurities present in the crude product. The vinyl proton shifts in the ^{1}H NMR spectrum under-integrated relative to what was expected for the product, supporting the hypothesis that auto-polymerization could have occurred. The final synthetic step for monomer **AAcGal** was repeated two more times with freshly distilled acryloyl chloride, DIPEA, and CH_2Cl_2. It has previously been stated in the literature that "The synthesis, isolation, and purification of glycomonomers is notoriously difficult." [36]

Due to the difficulty with replicating the synthesis of monomer **AAcGal**, synthesis of a new styrenic monomer, **SAcGal**, was explored (Scheme 2.3). In the first step, propargyl alcohol was deprotonated with sodium hydride in anhydrous tetrahydrofuran (THF) and substituted for the chlorine of 4-vinylbenzyl chloride, **3**, to afford compound **4**. Crude compound **1** underwent a CuAAC reaction with pure compound **4** to yield **SAcGal**. Based on ^{1}H NMR spectroscopy, **SAcGal** was pure after purification using a simple silica plug (Figure 2.2). IR spectroscopy showed no peak at ~2095 cm^{-1} indicating that there was no free azide remaining. The first step in the synthesis of **SAcGal** had a quantitative yield and the second step had a yield of 55%. **SAcGal** was stored with BHT to prevent auto-polymerization. The BHT inhibitor was removed using a silica plug immediately before polymerization.

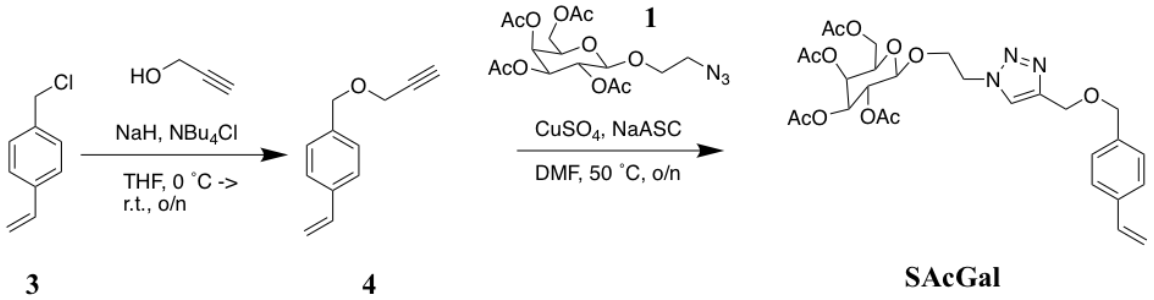

Scheme 2.3. Synthesis of the monomer **SAcGal**, a *β*-D-galactose pentaacetate functionalized styrenic monomer.

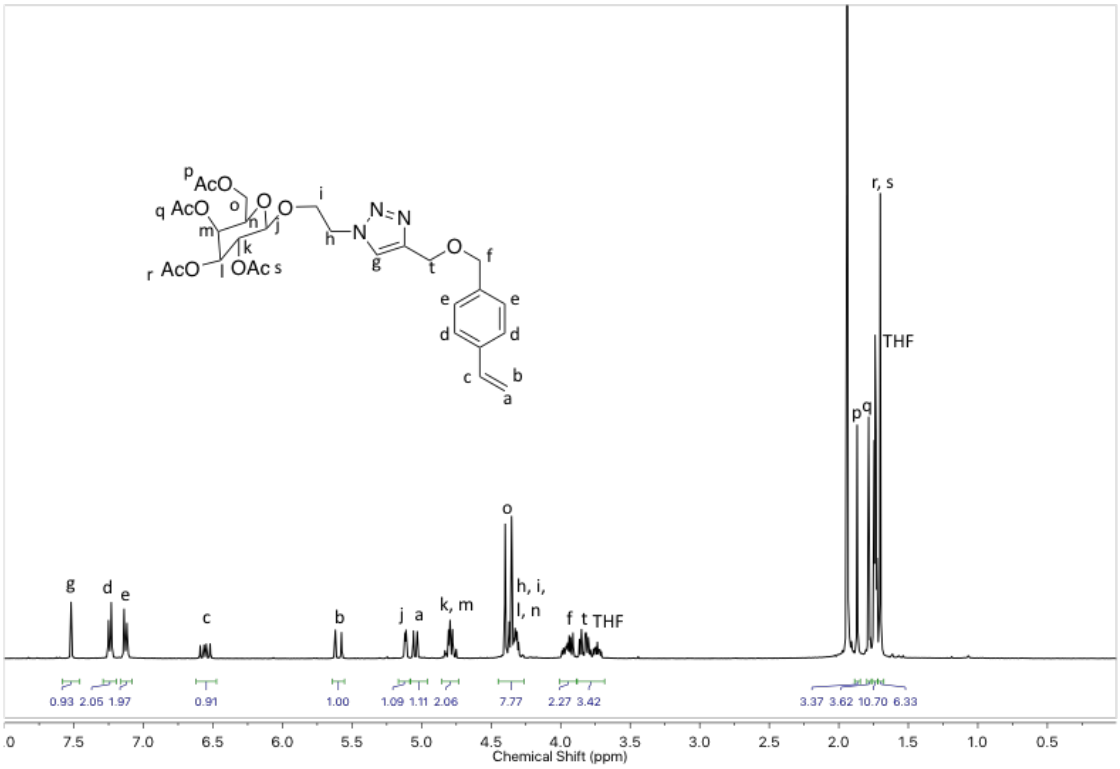

Figure 2.2. ^{1}H NMR spectrum of **SAcGal** (400 MHz, $CDCl_3$).

RAFT polymerization was selected because it enabled control over important glycopolymer properties including the molecular weight, dispersity, and end-groups. Exemplified by **PAGal$_9$** and **PAGal$_{19}$**, where the RAFT chain transfer agent (CTA) **5** contained an alkyne group (Scheme 2.4). Due to the nature of RAFT polymerization, the alkyne functionalized portion of the CTA would be incorporated into one of the glycopolymer terminal ends. This alkyne end-group could undergo CuAAC with the azide on the surface of the polymersomes to conjugate the glycopolymer to the polymersomes. The RAFT-mediated polymerization was initiated with azobisisobutyronitrile (AIBN), **6**, a thermal radical initiator. All free radical polymerization reactions are highly sensitive to $O_{2\,(g)}$, which can react with radicals. To remove oxygen, two methods were explored: Freeze-pump-thaw and bubbling N_2 gas through the polymerization mixture. Freeze-pump-thaw yielded the most consistent polymerization results likely due to inconsequential changes in concentration during the process. When bubbling N_2 gas through a polymerization mixture an ice bath is commonly used to reduce evaporation of the solvent, but a change in concentration and rate of polymerization was observed. To improve consistency freeze-pump-thaw was used. After degassing the polymerization mixture, it was heated at 70 ºC to initiate the polymerization.

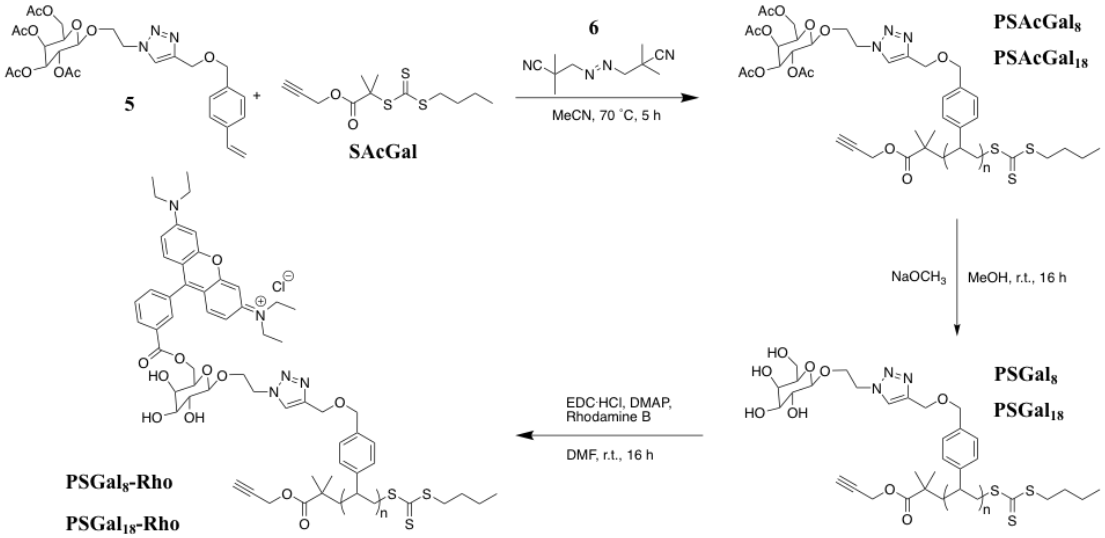

Scheme 2.4. RAFT-mediated polymerization of **SAcGal** and the subsequent deprotection and functionalization with Rhodamine B.

Similar to the initial glycopolymers **PAAcGal9** and **PAAcGal19**, two glycopolymers with different lengths were synthesized (Table 2.1). M_n, DP_n, and $Đ$ of the polymers were determined from SEC in THF relative to polystyrene standards, where calculating DP_n involved dividing the M_n by the molar mass of the repeat unit, 560 g/mol. End-group analysis by ^{1}H NMR spectroscopy was also used to determine a DP_n of the polymers. To determine DP_n the integration value of the CH_2 group next to the trithiocarbonate group (set to 2.0) was compared to the integration value of the saccharide's anomeric proton (Figure 2.3). The short protected glycopolymer **PSAcGal8** had an M_n of 4,700 g/mol, DP_n of ~8, and $Đ$ of 1.1 based on SEC, and an M_n of 6,700 g/mol and DP_n of ~12 based on ^{1}H NMR. The long protected glycopolymer **PSAcGal18** had an M_n of 10,000 g/mol, DP of ~18, and $Đ$ of 1.1 based on SEC, and an M_n of 21,000 and DP_n of ~38 based on ^{1}H NMR. The low dispersities determined by SEC demonstrate that the polymerizations were well controlled (Figure 2.4). It is unclear whether the M_n values determined by SEC or ^{1}H NMR are more representative of the true average molar mass for each polymer sample.

The values determined by SEC are limited by how similar the solvated conformation of **PSAcGal** is to the polystyrene calibration standards in THF. The M_n calculated using ^{1}H NMR spectroscopy is limited by the accuracy of the integration values, which are highly dependent on the conditions and parameters used to obtain the ^{1}H NMR spectrum and the subsequent data processing. The important conclusion that can be drawn based on the relative DP_ns from SEC and ^{1}H NMR spectroscopy, is that a shorter polymer, **PSAcGal$_8$**, and a longer polymer, **PSAcGal$_{18}$**, were successfully synthesized. Based on thermal analysis of **PSAcGal$_8$**, onset of decomposition temperature, T_o, was determined to be 315 ºC using thermogravimetric analysis (TGA), and the glass transition temperature was determined to be 70 ºC using differential scanning calorimetry (DSC).

Table 2.1. Summarized characterization results for short and long protected glycopolymer **PSAcGal**. Determined by [a] SEC, [b] TGA, [c] DSC, [d] ^{1}H NMR spectroscopy.

Polymer Sample	M_n (g/mol) [a]	DP_n[a]	$Đ$ [a]	T_o (ºC) [b]	T_g (ºC) [c]	M_n (g/mol) [d]	DP_n[d]
PSAcGal$_8$	4,700	8	1.1	315	70	6,700	12
PSAcGal$_{18}$	10,000	18	1.1			21,000	38

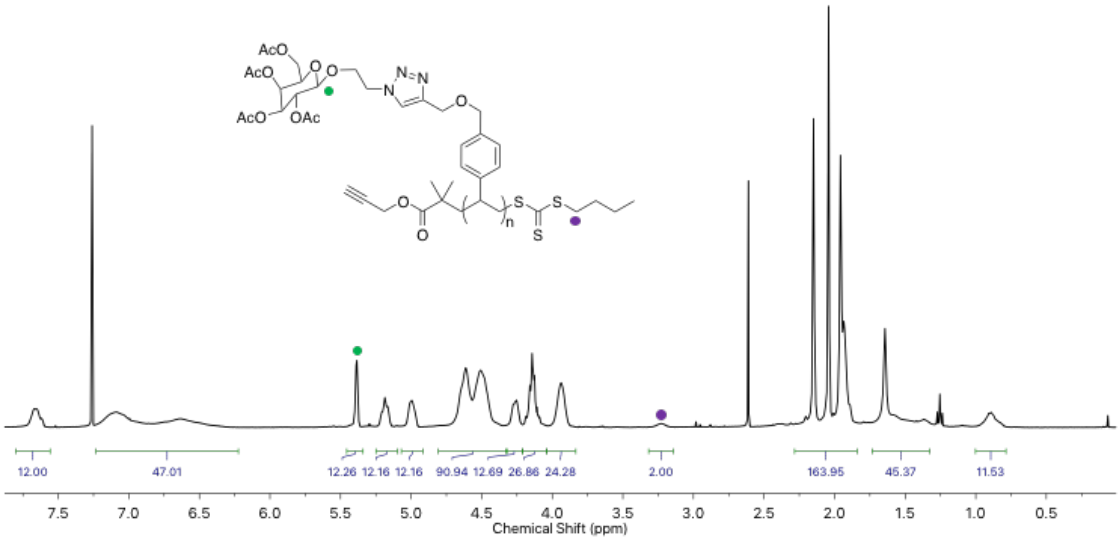

Figure 2.3. ^{1}H NMR spectrum (400 MHz, CDCl3) of $PSAcGal_8$ with the reference peaks for end-group analysis labelled.

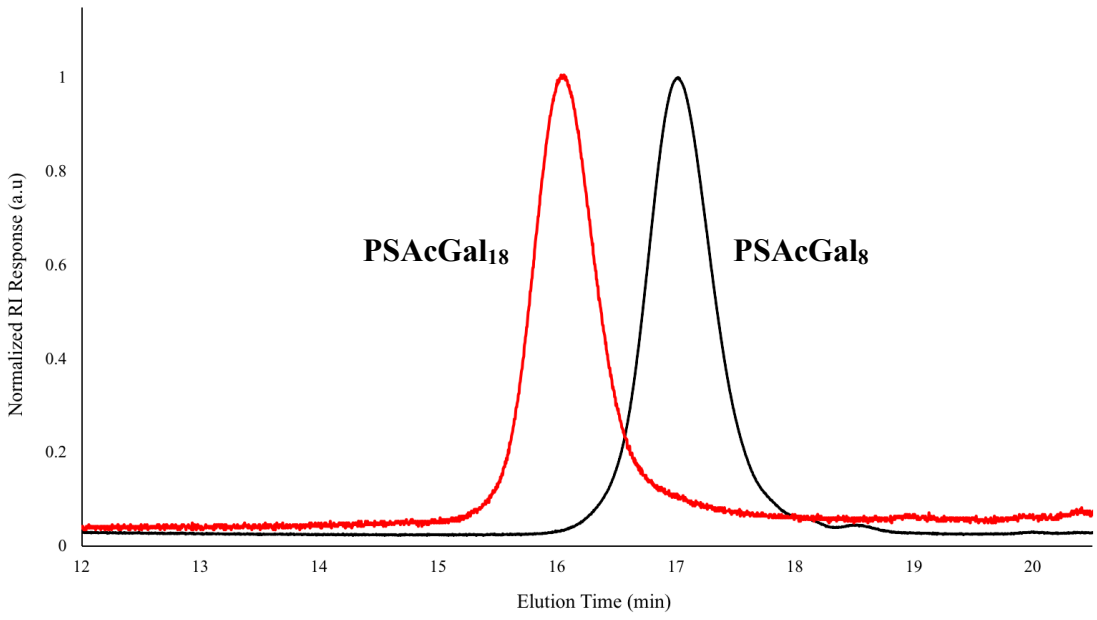

Figure 2.4. SEC traces of **$PSAcGal_8$** and **$PSAcGal_{18}$** in THF with refractive index detection.

The galactose functional groups on **PSAcGal$_8$** and **PSAcGal$_{18}$** were then deprotected, post-polymerization, using sodium methoxide in anhydrous methanol. ^{1}H NMR spectroscopy showed the disappearance of the acetyl protecting groups at ~2 ppm, which indicated successful deprotection of the hydroxy groups, yielding **PSGal$_8$** and **PSGal$_{18}$**. A small percentage of the exposed hydroxy groups, on each polymer **PSGal$_8$** and **PSGal$_{18}$**, were then functionalized with **rhodamine B** using the conditions described above for **PAGal$_9$** and **PAGal$_{19}$** (Scheme 2.4). The dye labeled glycopolymers, **PSGal$_8$-Rho** and **PSGal$_{18}$-Rho** had broad stryenic backbone peaks in aromatic region of the ^{1}H NMR spectrum, making it difficult to determine the exact number of conjugated rhodamine molecules.

2.2 Azide Functionalized PBD-PEO Polymersomes

The Gillies group has previously reported the preparation of azide-functionalized polymersomes from azide-terminated polybutadiene-*b*-poly(ethylene glycol) (PBD-PEG) block copolymers.[42] As previously reported, coupling of hydroxyl-terminated PBD-PEG (**PBD-PEG-OH**) with azidoacetic acid, **7**, using *N,N'*-dicyclohexylcarbodiimide (DCC) and DMAP allowed for the synthesis of **PBD-PEG-N$_3$** (Scheme 2.5). The polymersomes were assembled using an optimized thin-film hydration method. By varying the ratio of **PBD-PEG-OH** and **PBD-PEG-N$_3$**, the density of azides on the polymersome surface could be tuned. The **PBD-PEG-OH** and **PBD-PEG-N$_3$** were weighed out in the targeted ratio and dissolved in $CHCl_3$. The solvent was evaporated under a stream of nitrogen, then the vial was put under high-vacuum for 16 hours to yield a thin-film. The film was hydrated with Milli-Q water at 46 °C overnight, then stirred rapidly at 46 °C for 16 hours to afford polymersomes. The initial compositions tested were 10% and 100% **PBD-PEG-N$_3$**, with the remainder being **PBD-PEG-OH**. Polymersomes were imaged using confocal laser scanning microscopy (CLSM) by incorporating nile red, a fluorescent probe, into the hydrophobic membrane of the polymersome. This was accomplished by the addition of 0.1 weight percent (wt%) of nile red to the polymer in $CHCl_3$ during the polymer film

preparation. CLSM images of the PBD-PEG assemblies confirmed the vesicle morphology (Figure 2.5 (a)). The polymersomes were approximately 3-5 μm in size.

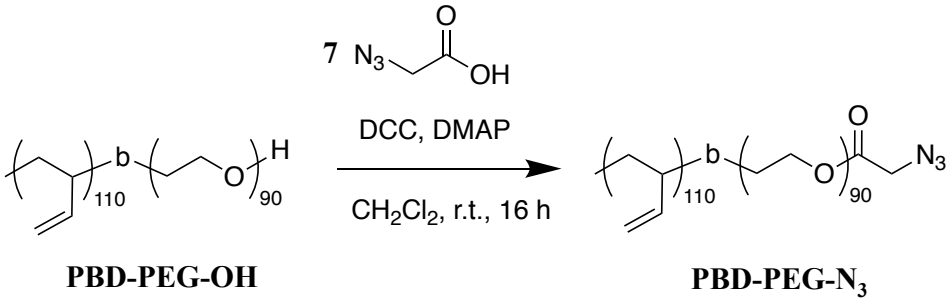

PBD-PEG-OH **PBD-PEG-N_3**

Scheme 2.5. Synthesis of azide functionalized PBD-PEG (**PBD-PEG-N_3**).

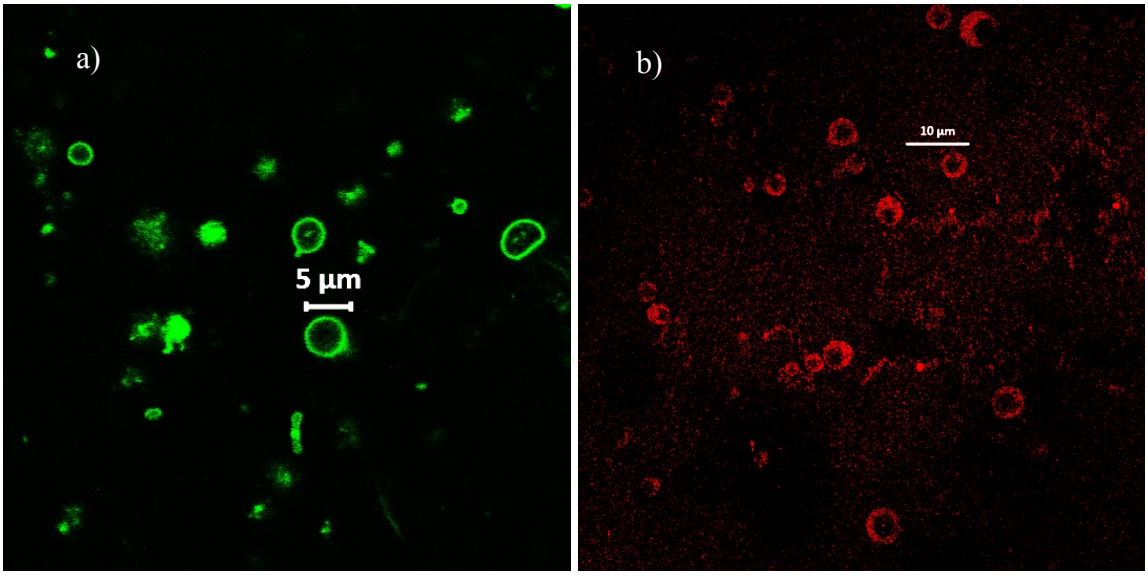

Figure 2.5. CLSM images of 100% **PBD-PEG-N_3** polymersomes: a) loaded with nile red and (b) with rhodamine functionalized glycopolymer, **$PAGal_{19}$-Rho**, conjugated to the surface.

Next, polymersomes containing 10% and 100% **PBD-PEG-N_3** were assembled without nile red. These assemblies were reacted with rhodamine functionalized polymers using

CuAAC by adding $CuSO_4$, (+)-sodium L-ascorbate, bathophenanthrolinedisulfonic acid disodium salt hydrate (BPS), and either **PAGal$_9$-Rho** or **PAGal$_{19}$-Rho** to the polymersome solution (Scheme 2.6). After the CuAAC reaction, unreacted glycopolymer, $CuSO_4$, (+)-sodium L-ascorbate, and DPS were removed by dialysis against water using a 50,000 MWCO membrane. A control experiment, where no $CuSO_4$ was added to the reaction mixture, was conducted to confirm that any unreacted dyed glycopolymer was removed using dialysis. The glycopolymer coated assemblies were imaged using CLSM. Images indicated that the vesicle morphology was retained post-functionalization with **PAGal$_9$-Rho** or **PAGal$_{19}$-Rho** at 10% and 100% surface functionalization densities (Figure 2.5 (b)). **PSGal-Rho** polymers were conjugated to **PBD-PEG-N$_3$** polymersomes using the same methods above. CLSM images similarly indicate that vesicle morphology was retained post-functionalized with **PSGal$_8$-Rho** at 10% and 100% surface functionalization densities (Figure 2.6). **PSGal$_{18}$-Rho** functionalized assemblies were not able to be successfully imaged at either surface density.

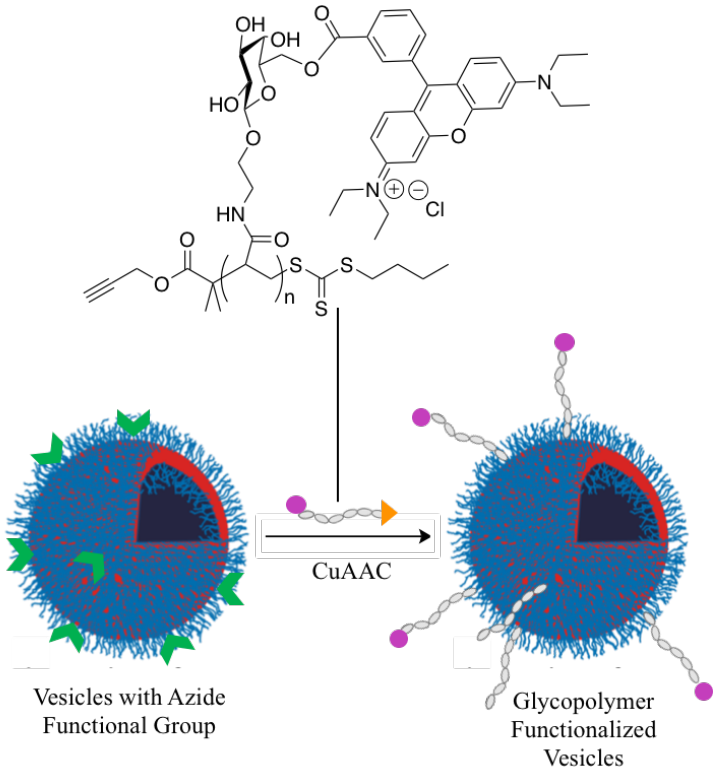

Scheme 2.6. Preparation of **PAGal-Rho**-functionalized PBD-PEG polymersomes**.**

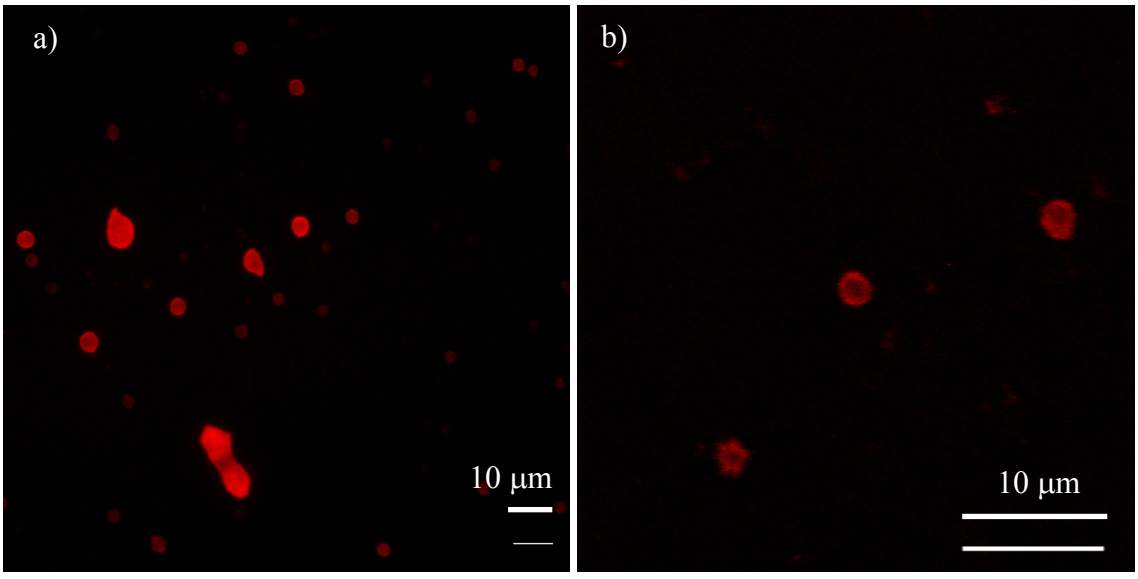

Figure 2.6. CLSM image of (a) 10% **PBD-PEG-N3** and (b) 100% **PBD-PEG-N3** polymersomes conjugated with **PSGal$_9$-Rho**.

2.3 Quantification of CuAAC with Azide Functionalized PBD-PEO Polymersomes

PBD-PEG polymersomes functionalized with dye labelled glycopolymers were used to determine the percent of surface functionalization for **PAGal$_9$-Rho**, **PAGal$_{19}$-Rho**, and **PSGal$_8$-Rho**. Fluorescence spectroscopy was used to determine the concentration of rhodamine labelled glycopolymer present after the reaction and purification of the polymersomes by dialysis. This was determined by comparing the fluorescence counts of the decorated polymersomes in dimethyl sulfoxide (DMSO) to the fluorescence counts of a calibration curve for the corresponding dye labelled polymer **PAGal$_9$-Rho**, **PAGal$_{19}$-Rho**, and **PSGal$_8$-Rho** in DMSO. A calibration curve was created for each **PAGal$_9$-Rho**, **PAGal$_{19}$-Rho**, and **PSGal$_8$-Rho** because they had different percentages of dye functionalization. The results indicated that polymersome samples prepared from 10 wt% of **PBD-PEG-N$_3$** had a higher degree of N_3 groups functionalized with dye labelled glycopolymers **PAGal$_9$-Rho** and **PAGal$_{19}$-Rho** (Table 2.2). The lower degree of N_3 groups functionalized on the 100 wt% of **PBD-PEG-N$_3$** polymersome samples may be due to the steric hindrance that is associated with functionalizing every N_3 group. Glycopolymer length appeared to have no significant effect on the percentage of functionalized azide groups. It should be noted that 100% functionalization would mean that 50% of all present azide groups had reacted. The reference of 50% is selected because it is assumed that 50% of the azide groups would be on the surface of the interior cavity of the polymersome and unavailable to react with the glycopolymer. A previous study on the amount of azide groups available to react on the surface of PBD-PEG polymersomes indicated that the above assumption is reasonable.[39,42]

Table 2.2. Table summarizing the percentage of functionalized azide groups relative to the total number of available azide groups.

	10% of PBD-PEG-N_3 (%)	100% of PBD-PEG-N_3 (%)
PAGal$_9$-Rho	82	74
PAGal$_{19}$-Rho	90	70
PSGal$_8$-Rho		89

2.4 Difficulties in the reproducibility of polymersome preparation

At this stage in the project, difficulties arose with the reproducibility of the self-assembled polymersomes. The irreproducible nature of the polymersome formation may be attributed to the potential crosslinking of free double bonds in the PBD block of the **PBD-PEG** block copolymers. The recent ^{1}H NMR spectrum of the **PBD-PEG** block copolymer appeared similar to the spectrum recorded a year earlier. A large decrease in the integration of the vinyl peaks at around 5.4 ppm would have been a clear indication of crosslinking. However small decreases, or a small amount of crosslinking, couldn't be accurately assessed due to the broad nature of polymer ^{1}H NMR peaks. Minor changes in the chemical properties of the polymer sample, even by small amounts of crosslinking or oxidation, could disrupt the self-assembly of polymersomes. It should be noted that small, unidentifiable changes to the self-assembly technique, could also be responsible for the change in observed morphology. Polymer Source, the polymer provider, discontinued the exact polymer sample the Gillies group had previously used, so a fresh batch of polymer could not be ordered. Ultimately, due to the issues with reproducibility and availability, a more robust system for forming polymersomes using a polymer we could make in the lab was selected for future studies.

2.5 Azide Functionalized PEG-PEtG-PEG Polymersomes

Poly(ethyl glyoxylate) (PEtG) is a hydrophobic polymer that has been shown to self-assemble when coupled with PEG. The Gillies group has previously shown that **MeO-PEG-PEtG-PEG-OMe** triblock polymers self-assembled into vesicle morphologies when the length of each terminal PEG was 750 g/mol and the PEtG block was ~63,000 g/mol.[45] In order to produce functionalizable polymersomes of PEtG and PEG, azides were incorporated onto the triblock termini (**N_3-PEG-PEtG$_{UV}$-PEG-N_3**). To vary the degree of surface functionalization, a similar triblock copolymer with methyl ether terminal groups was also prepared (**MeO-PEG-PEtG$_{UV}$-PEG-OMe**) (Figure 2.7).

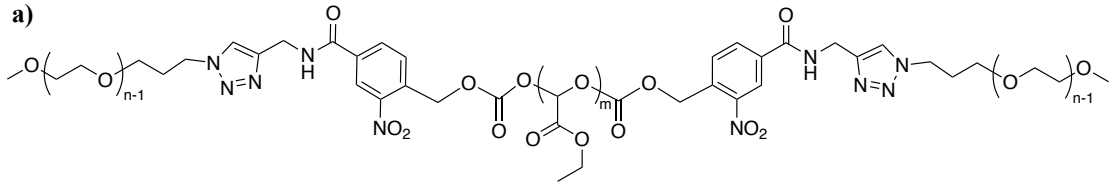

MeO-PEG-PEtG$_{UV}$-PEG-OMe (550) (m = 530, n = 13)

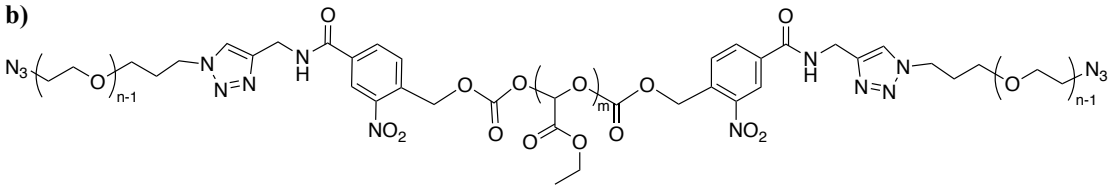

N_3-PEG-PEtG$_{UV}$-PEG-N_3 (600) (m = 530, n = 14),

N_3-PEG-PEtG$_{UV}$-PEG-N_3 (1000) (m = 530, n = 23)

Figure 2.7. Structures of the target triblock copolymers (a) **MeO-PEG-PEtG$_{UV}$-PEG-OMe (550)** and (b) **N3-PEG-PEtG$_{UV}$-PEG-N3 (600)** and **N3-PEG-PEtG$_{UV}$-PEG-N3 (1000)**.

The first step in the synthesis of the triblocks was making the PEG portions. Compound **8** (M_n = 550 g/mol) and **11** (M_n = 600 g/mol) and **12** (M_n = 1,000 g/mol)**,** were reacted with mesyl chloride, **9**, to convert the alcohol into a good leaving group (Scheme 2.7). The mesylated PEGs, **10, 13,** and **14**, were then reacted with sodium azide to afford the corresponding azide-terminated PEGs **MeO-PEG-N$_3$ (550)**, **N$_3$-PEG-N$_3$ (600),** and **N$_3$-PEG-N$_3$ (1000)**. ^{1}H NMR spectroscopy indicated the successful substitution of the mesyl group with an azide group in all cases. The substitution was indicated by the disappearance of the methyl peak of the mesyl group at 3.1 ppm. In addition, IR spectroscopy confirmed the presence of an azide peak in **MeO-PEG-N$_3$ (550)**, **N$_3$-PEG-N$_3$ (600),** and **N$_3$-PEG-N$_3$ (1000)** at ~2098 cm^{-1}. Two PEG di-azide compounds of different lengths were made to test the effect of PEG length on self-assembly. Previous examples of **MeO-PEG-PEtG-PEG-OMe** that could form polymersomes used PEG with an M_n of 750 g/mol, but a diol form with a similar M_n was not commercially available.

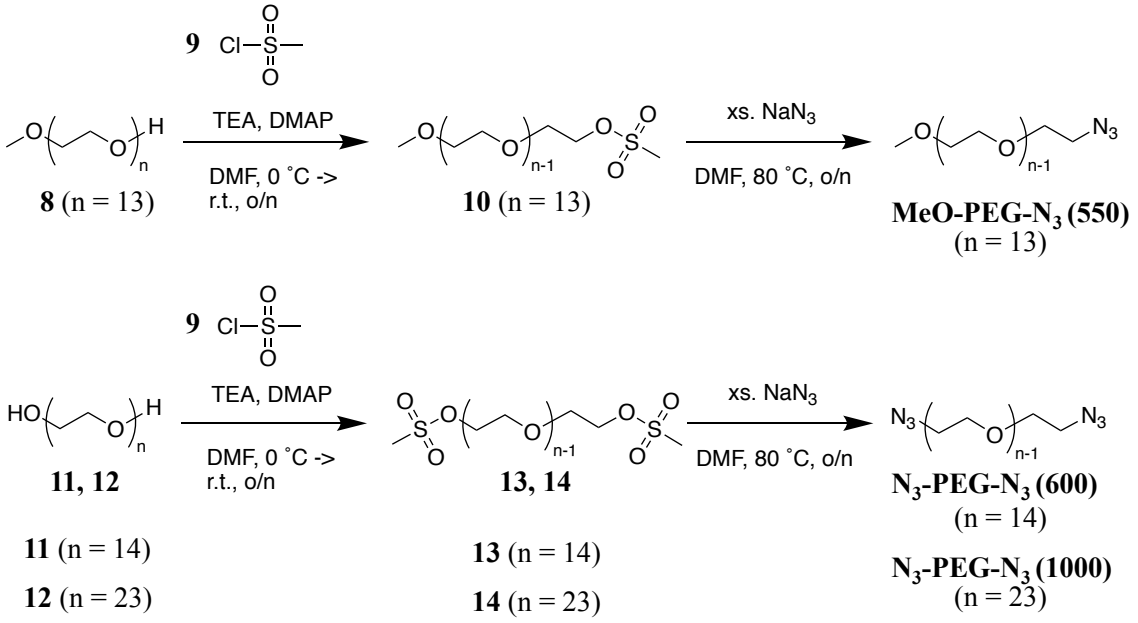

Scheme 2.7. Synthesis of (a) mono-azide terminated PEG, **MeO-PEG-N3**, and (b) di-azide terminated PEG, **N3-PEG-N3**.

The PEtG portion of the triblock, **PEtG$_{UV}$** (Scheme 2.8) with alkyne terminal groups was previously prepared and had an M_n of 72,000 and $Đ$ of 1.9. It is important to note that the end-cap used is reactive with UV light, and this could be taken advantage of to trigger polymer degradation. However, it was not the goal of the current work to take advantage of the degradable properties. CuAAC was used to couple the PEGs to the **PEtG$_{UV}$** (Scheme 2.8). For the reaction between PEtG and both **N$_3$-PEG-N$_3$** compounds, a molar excess of up to 100 times was used. It would have required a multi-step synthesis to form a unilaterally functionalized PEG moiety. Instead, by using a large excess of **N$_3$-PEG-N$_3$**, a statistical mixture favouring the exclusive reaction of **N$_3$-PEG-N$_3$** and **PEtG$_{UV}$** alkyne was used. This approach minimized the reaction of a single **N$_3$-PEG-N$_3$** with two different alkyne terminated **PEtG$_{UV}$** polymers, which prevented the potential formation of a copolymer containing five or more blocks. The resulting triblock polymers were characterized using ^{1}H NMR spectroscopy, Fourier-transform infrared spectroscopy (FT-IR), and SEC. ^{1}H NMR spectroscopy indicated that the coupling of all three PEG compounds to **PEtG$_{UV}$** was successful, based on the appearance of the expected PEG peaks at around 3.64 ppm (Figure 2.8). FT-IR did not show any sharp peaks at ~2098 cm^{-1}, which are expected if there is unreacted PEG azide in the sample (Figure 2.9). However, the lack of an azide related peak could have been due to the relatively small amount of azide compared to the amount of polymer, thus, SEC was used to confirm that only trace amounts of PEG were present and the respective peaks in the ^{1}H NMR spectrum are not from excess unreacted PEG (Figure 2.10). It was concluded that the CuAAC reaction and subsequent purification was successful.

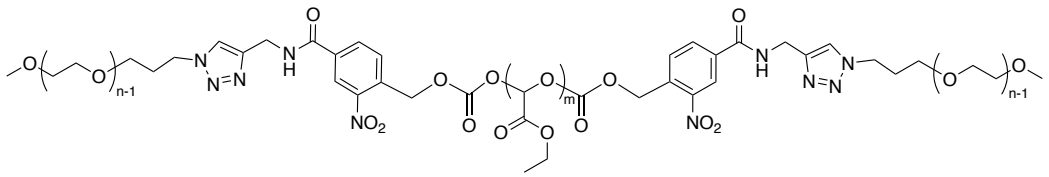

MeO-PEG-PEtG$_{UV}$-PEG-OMe (550) (m = 530, n = 13)

MeO-PEG-N$_3$ (550)

$CuSO_4$, NaASC, DMF, 50 ˚C, o/n

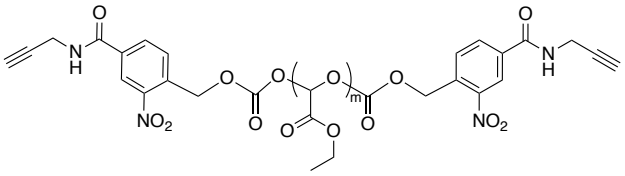

PEtG$_{UV}$

N$_3$-PEG-N$_3$ (600)
N$_3$-PEG-N$_3$ (1000)

100 equiv. xs.

$CuSO_4$, NaASC, DMF, 50 ˚C, o/n

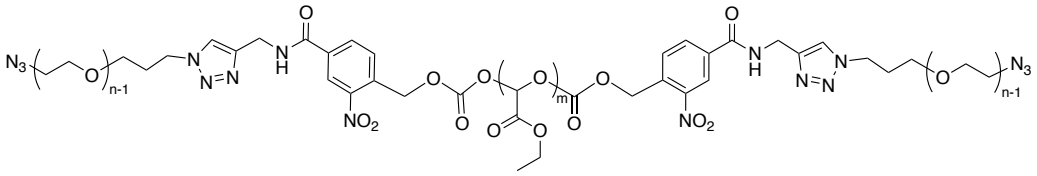

N$_3$-PEG-PEtG$_{UV}$-PEG-N$_3$ (600) (m = 530, n = 14)
N$_3$-PEG-PEtG$_{UV}$-PEG-N$_3$ (1000) (m = 530, n = 23)

Scheme 2.8. Synthesis of **MeO-PEG-PEtG$_{UV}$-PEG-OMe (550)** and (b) **N3-PEG-PEtG$_{UV}$-PEG-N3 (600)**.

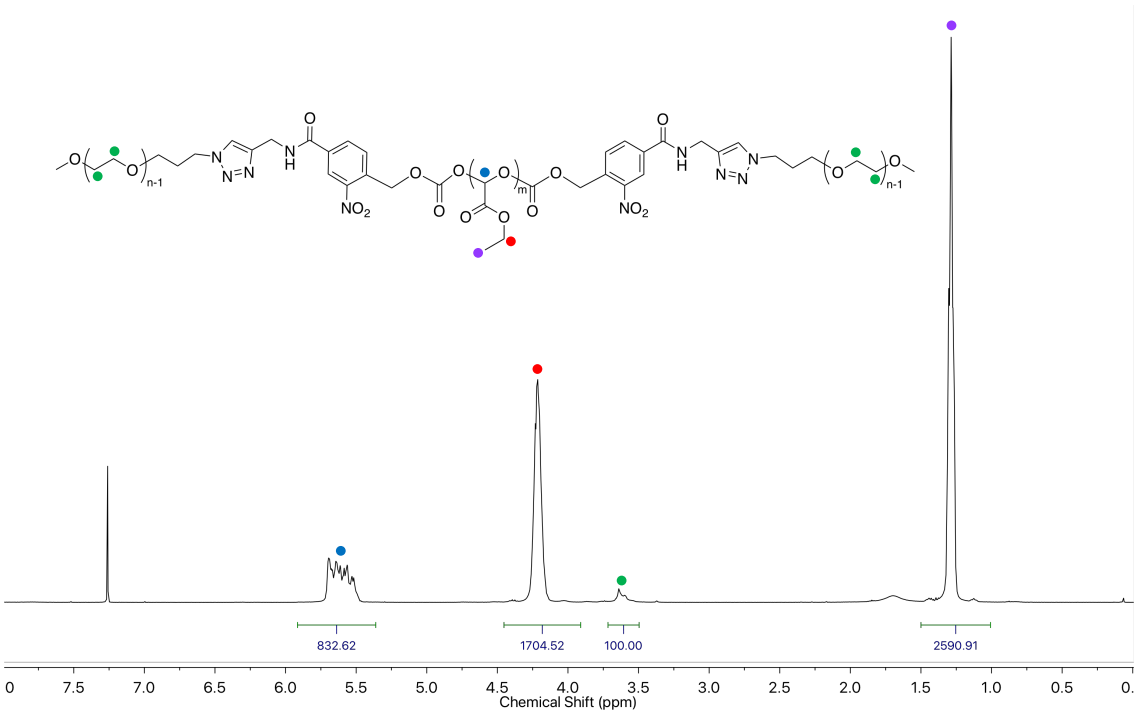

Figure 2.8. ^{1}H NMR spectrum (400 MHz, CDCl3) of **MeO-PEG-PEtG$_{UV}$-PEG-MeO (550)**.

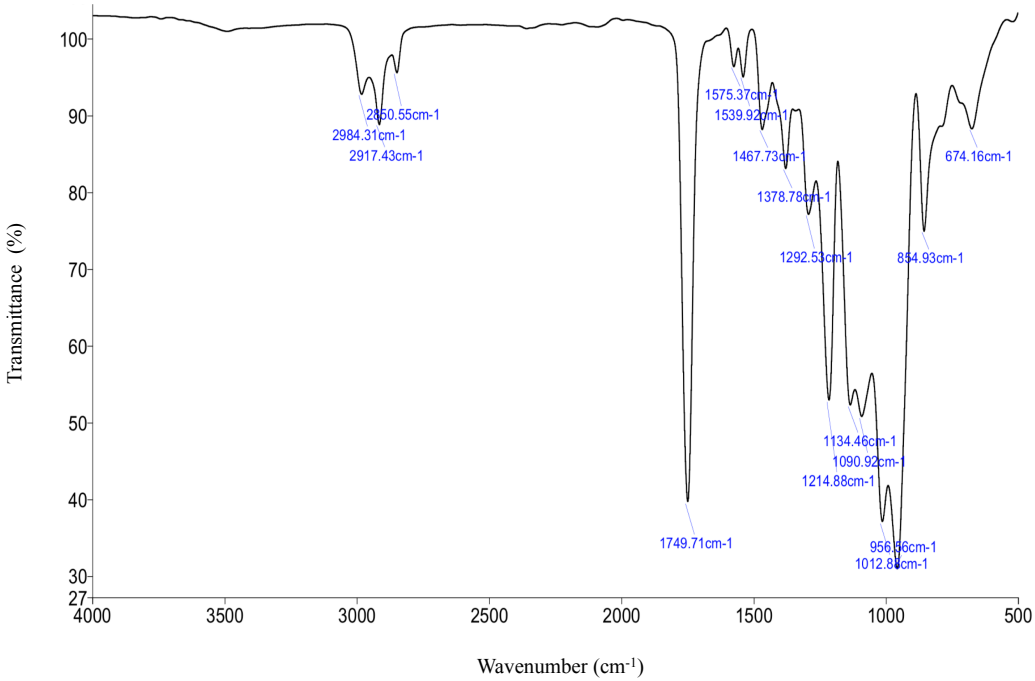

Figure 2.9. FT-IR spectrum of **MeO-PEG-PEtG$_{UV}$-PEG-MeO (550).**

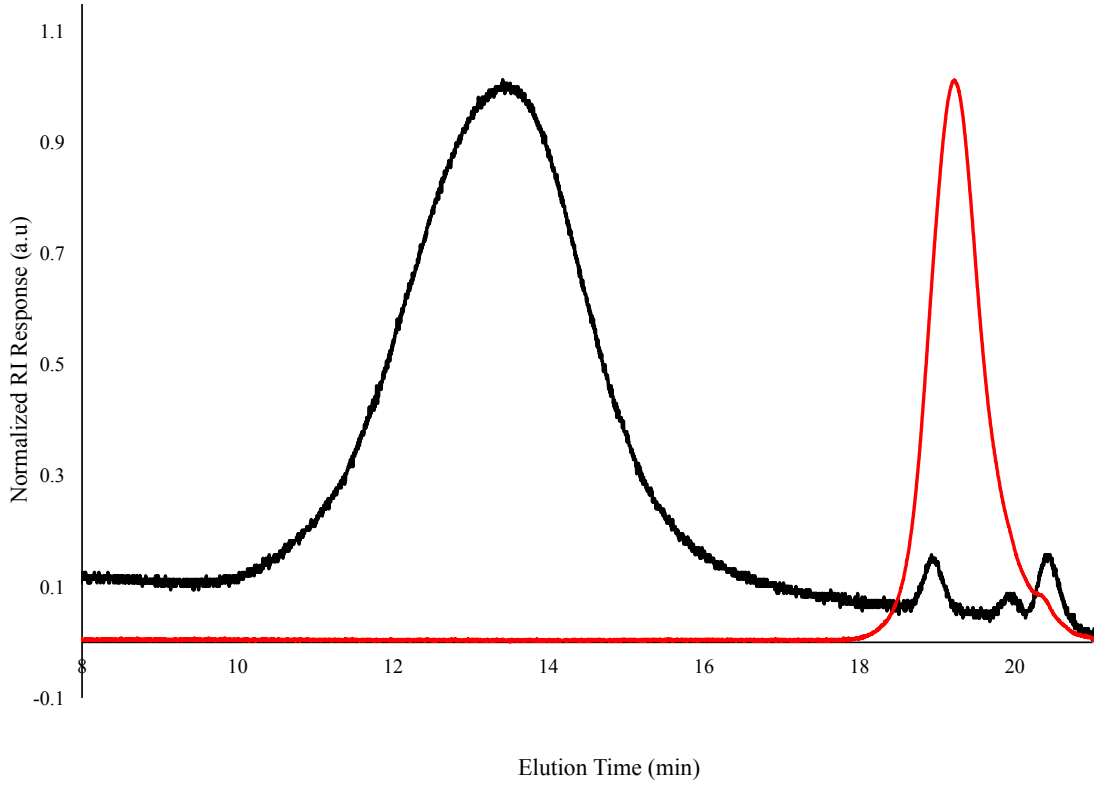

Figure 2.10. Overlay of the SEC traces for (a) **MeO-PEG-PEtG$_{UV}$-PEG-MeO (550)** and (b) **MeO-PEG-N3.**

Various ratios of polymers **MeO-PEG-PEtG$_{UV}$-PEG-MeO (550)** and **N$_3$-PEG-PEtG$_{UV}$-PEG-N$_3$ (600)** were self-assembled to alter the surface azide density. In order to visualize the resulting assemblies, they were loaded with perylene, a hydrophobic fluorescent probe that excites at 410 nm. This probe was selected because the excitation and emission curves do not overlap with the respective curves of the rhodamine labelled glycopolymers, **PSGal-Rho**, allowing for direct quantification by fluorescence microscopy after imaging with CLSM. Unfortunately, the self-assembly of **MeO-PEG-PEtG$_{UV}$-PEG-MeO (550)**, **N$_3$-PEG-PEtG$_{UV}$-PEG-N$_3$ (600),** or **PEG-PEtG$_{UV}$-PEG-N$_3$ (1000)** at any ratio (10%, 20%, or 50%) initially lead to small particles could be imaged by CLSM, but no distinguishable membrane structure typical of vesicle morphology was observed (Figure 2.11). Transmission electron microscopy (TEM) is commonly used to visualize the morphology of smaller particles, but unfortunately the instrument was unavailable for an extended period of time, which prevented analysis by TEM. The self-

assembly of samples containing exclusively polymer **MeO-PEG-PEtG$_{UV}$-PEG-MeO (550)**, **N$_3$-PEG-PEtG$_{UV}$-PEG-N$_3$ (600),** or **PEG-PEtG$_{UV}$-PEG-N$_3$ (1000)** were tested to determine if large polymersomes could be formed by a single triblock, rather than a mixture. The results indicated that small particles formed for all three triblock samples. The z-average diameter of the assemblies **MeO-PEG-PEtG$_{UV}$-PEG-MeO (550)** and **N$_3$-PEG-PEtG$_{UV}$-PEG-N$_3$ (600)** were determined to be 182 nm with a PDI of 0.06 and 155.9 with a PDI of 0.143 by DLS. The PDI for a sample to be considered monodisperse must be less than 0.2. Thus, the assemblies of **MeO-PEG-PEtG$_{UV}$-PEG-MeO (550)** and **N$_3$-PEG-PEtG$_{UV}$-PEG-N$_3$ (600)** are both monodisperse and could be useful for functionalization depending on the morphology determined by TEM imaging in the future.

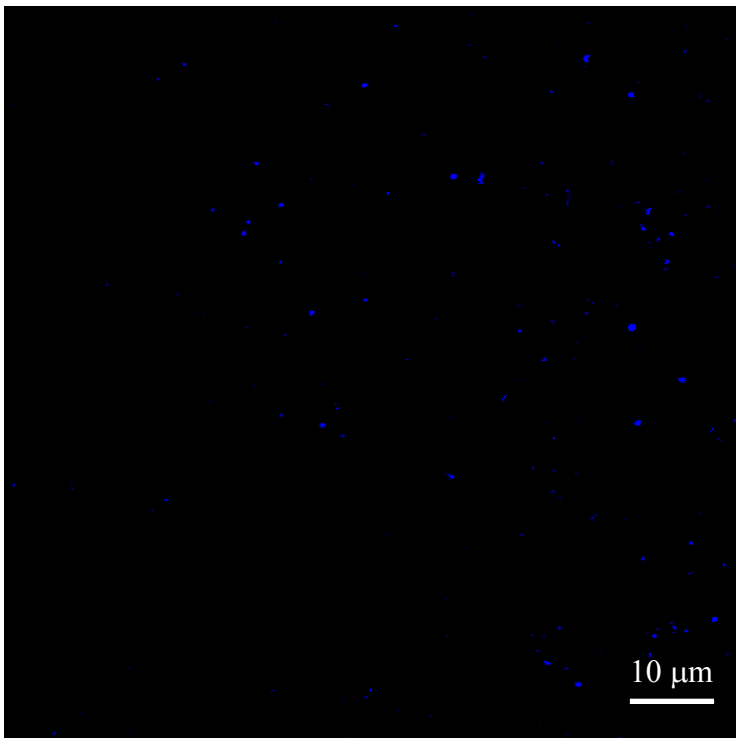

Figure 2.11. CLSM images of the **PEG-PEtG$_{UV}$-PEG-N3 (1000)** suspension, showing that small particles were obtained.

A **MeO-PEG-PEtG$_{Thermo}$-PEG-OMe** triblock polymer containing a **PEtG$_{Thermo}$** block with an M_n of 63,000 g/mol and PEG with an M_n of 750 g/mol, and a thermos-responsive end-cap (Figure 2.12) was shown by the Gillies group to form large polymersomes that could be visualized by CLSM. To take advantage of this polymersome forming triblock polymer and form large easily visualized polymersomes coated with azide groups, **MeO-PEG-PEtG$_{Thermo}$-PEG-OMe** was mixed with **PEG-PEtG$_{UV}$-PEG-N$_3$ (1000)**. The ratios selected were 10%, 30%, and 50% **PEG-PEtG$_{UV}$-PEG-N$_3$ (1000)** to **MeO-PEG-PEtG$_{Thermo}$-PEG-OMe**. Preliminary CLSM images of the mixed suspensions indicated larger vesicle and smaller particles morphologies were present (Figure 2.13). Similar mixed morphologies were observed for all polymer ratios. By optimizing both the mixing ratios and methods used to form the assemblies, mixing **MeO-PEG-PEtG$_{Thermo}$-PEG-OMe** and **PEG-PEtG$_{UV}$-PEG-N$_3$ (1000)** may present a viable route to achieving reproducible and functionalizable polymersomes.

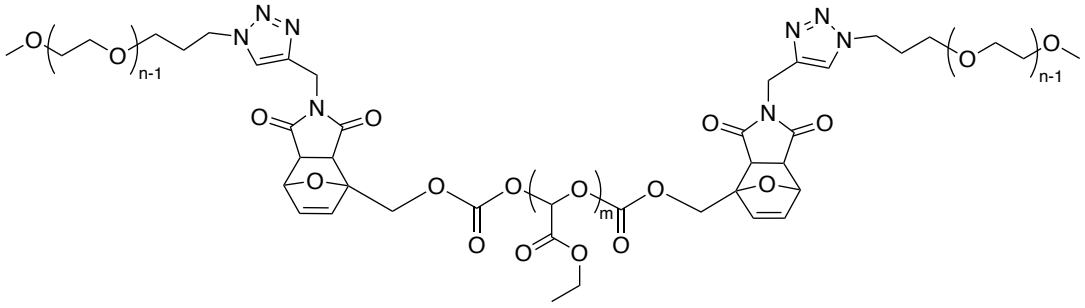

MeO-PEG-PEtG$_{Thermo}$-PEG-OMe (m = 618, n = 17)

Figure 2.12. Chemical structure of **MeO-PEG-PEtG$_{Thermo}$-PEG-OMe.**

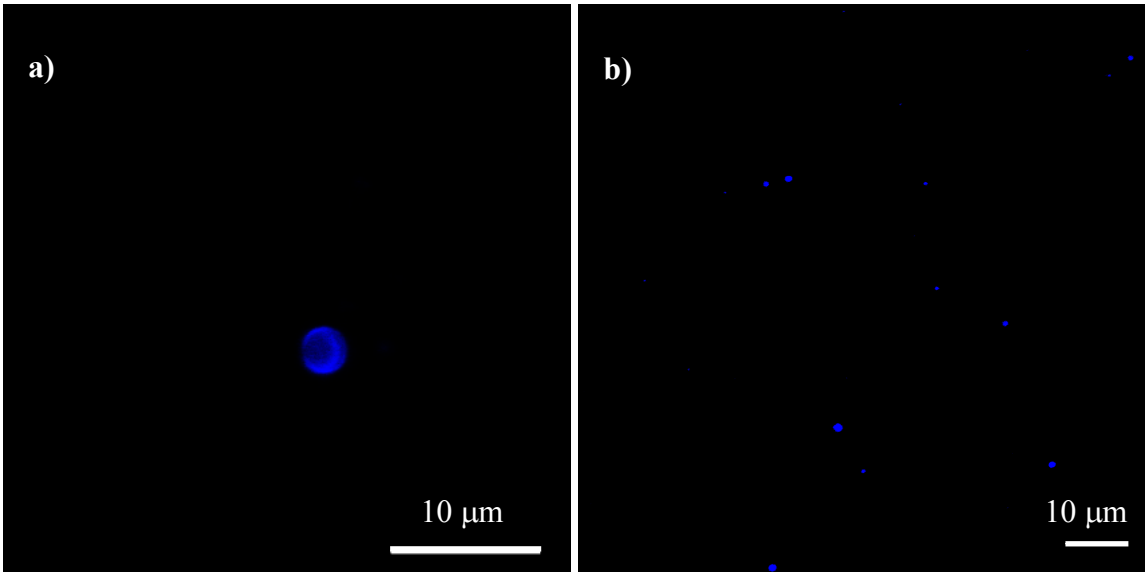

Figure 2.13. (a) Large vesicle morphology and (b) small particles observed within the same 10 wt% **N3-PEG-PEtG$_{UV}$-PEG-N3 (1000)** 90 wt% **MeO-PEG-PEtG$_{Thermo}$-PEG-OMe (750)** nanoparticle suspension.

Chapter 3

3 Experimental

General Procedures and Methods. Compounds **1**[46], **2, 5 ,7**[44], **4**[47], **10**[48], **13**[48] and **14**[48] were prepared as previously reported. **PEtG$_{UV}$** had an M_n = 54,000 g/mol and $Đ$ = 2.2 by SEC in THF. **PEtG$_{Thermo}$** had an M_n = 63,000 g/mol and $Đ$ = 2.0 by SEC in THF. DIPEA and dichloromethane were distilled from calcium hydride before use. Anhydrous THF was obtained from a solvent purification system using aluminum oxide columns. All other solvents were purchased from Caledon Labs. All the other chemicals were reagent grade and used without further purification. NMR spectra were obtained on 400 or 600 MHz Varian Inova spectrometers (Agilent Tech., Santa Clara, CA). NMR chemical shifts (δ) are reported in ppm and are calibrated against the residual solvent signals of $CDCl_3$ (δ 7.27; 77.4), CD_3CN (δ 1.94; 116.4), d6-DMSO (δ 2.50; 40.8), or D_2O (δ 4.75). Size exclusion chromatography (SEC) was performed using a Viscotek GPC Max VE2001 solvent module (Agilent Tech.), a Viscotek VE3580 RI detector operating at 30 °C, two Agilent Polypore (300 × 7.5 mm) columns connected, and a Polypore guard column (50 × 7.5 mm). THF (glass distilled grade) was used as the eluent. A calibration curve was obtained from polystyrene standards. Dialysis was performed using Spectra/Por 6 regenerated cellulose membranes from Spectrum Laboratories (Rancho Dominguez, CA, USA). Fourier-transform infrared (FT-IR) spectra were obtained in attenuated total reflectance (ATR) mode using a PerkinElmer UATR Spectrum Two, with bulk material deposited on the diamond. Ultrapure water was obtained from a Barnstead EASYpure II system. The Z-average diameters of the polymersome assemblies were measured by dynamic light scattering (DLS) using a Zetasizer Nano Series ZS instrument from Malvern Instruments, at room temperature (25 ºC) in a 1 cm path length low volume (1 mL) polystyrene cuvette at a polymer concentration of 0.8 mg/mL. Fluorescence spectra were obtained using a QM-SE spectrometer from Photon Technology International (PTI). Thermogravimetric analyses (TGA) were performed on a TGA Q50 from TA Instruments. The heating rate was 10。C /min between 15-1000 ºC under $N_{2\ (g)}$.

Differential scanning calorimetry (DSC) was performed using a Q2000 from TA Instruments. The heating/cooling rate was 10 ºC/min from -70 to +150 ºC. Glass transition temperatures (T_g) were obtained from the third heating cycle.

Synthesis of SAcGal. 1-O-2-Azidoethyl-β-D-galactose tetraacetate[46] (19 g, 46 mmol, 1.0 equiv.) was dissolved in minimal dimethylformamide (DMF) with stirring. Sequentially, $CuSO_4$ (0.90 g, 4.6 mmol, 0.10 equiv.), (+)-Sodium L-ascorbate (2.7 g, 4.6 mmol, 0.10 equiv.), and compound **4** (9.4 g, 55 mmol, 1.2 equiv.) dissolved in minimal DMF, were added to the flask. 450 mL of 4:1 DMF:water was added to the mixture and it was heated with rapid stirring at 50 °C overnight. The reaction mixture was concentrated *in vacuo* and the crude product dissolved in CH_2Cl_2 (500 mL), washed with water, brine (300 mL each). The organic layer was dried with $MgSO_4$, filtered and concentrated. The crude mixture was precipitated twice from minimal THF into cold pentane and residual solvent removed under high vacuum to yield **SAcGal** (14.5 g, 55%). 1 g of BHT in 20 mL of dichloromethane was added to the **SAcGal** and the solution was stored in a -20 ºC freezer to prevent polymerization. ^{1}H NMR (400 MHz, CD_3CN): δ_{ppm} 7.52 (s, 1H), 7.24 (d, 2H, J = 8.0 Hz), 7.13 (d, 2H, J = 8.0 Hz), 6.56 (dd, 1H, J = 12.0, 16.0 Hz), 5.60 (d, 1H, J = 16.0 Hz), 5.12 (d, 1H, J = 4 Hz), 5.05 (d, 1H, J = 12.0 Hz), 4.83-4.75 (m, 2H), 4.40-4.30 (m, 8H), 3.99-3.91 (m, 2H), 1.70 (s, 6H), 1.87 (s, 3H), 1.79 (s, 3H), 1.71 (s, 6H). FT-IR (cm^{-1}, film from CH_2Cl_2): 2867, 1743, 1368, 1218, and 1046 cm^{-1}.

Synthesis of $PSAcGal_8$ and the general procedure for the polymerization of SAcGal. Before use, **SAcGal** containing BHT was dissolved in CH_2Cl_2 and loaded onto a silica plug. BHT was eluted with CH_2Cl_2 and discarded. The monomer was then eluted with 100% methanol. The methanol was removed *in vacuo* and the purified **SAcGal** (1.2 g, 2.2 mmol, 13 equiv.), CTA (compound **5**) (50 mg, 170 μmol, 1.0 equiv.), and AIBN, **6**, (9.4 mg, 57 μmol, 0.33 equiv.) were deposited in a reaction tube and dissolved in acetonitrile (1 mL). The polymerization mixture was subjected to four cycles of freeze-pump-thaw. A freeze-pump-thaw cycle began with freezing the polymerization mixture using liquid nitrogen under a positive pressure of $N_{2\ (g)}$. Once the sample was frozen, the flask was placed under active high vacuum for 5 min, with the flask remaining in liquid nitrogen. The flask was removed from the liquid nitrogen and placed under static vacuum, until the

sample was thawed. The sample would then be re-frozen, and the cycle repeated the desired number of times. After being placed under positive pressure of $N_{2\ (g)}$, the mixture was heated to 75 °C and stirred rapidly for 36 h. The polymerization mixture was allowed to cool to room temperature and concentrated. The crude polymer was dissolved in DMF (2 mL) and dialyzed against 1 L of DMF using a 2,000 g/mol MWCO membrane for 18 h. The solution was concentrated yielding **PSAcGal$_8$** (910 mg, 76%). ^{1}H NMR (400 MHz, $CDCl_3$): δ_{ppm} 7.65 (br s, 1H), 7.23-6.30 (br, 4H), 5.38 (br s, 1H), 5.19 (br, 1H), 5.00 (br s, 1H), 4.76-4.35(br, 7H), 4.26 (s, 1H), 4.26 (m, 2H), 3.94 (br s, 2H), 2.15-1.96 (m, 13H), 1.72-1.30 (br, 4H), 0.89 (br s, 1H). SEC: M_n = 4,700 g/mol, M_w = 5,300 g/mol, $Đ$ = 1.1.

Synthesis of PSAcGal$_{18}$. The polymer was synthesized by the same procedure described for **PSAcGal$_8$** except for the following changes. Purified **SAcGal** (1.2 g, 2.2 mmol, 45 equiv.), CTA (compound **5**) (14 mg, 48 μmol, 1.0 equiv.), and AIBN (2.6 mg, 16 μmol, 0.33 equiv.) were deposited in a reaction tube and dissolved in acetonitrile (1 mL). The polymerization mixture was heated at 75 ºC with rapid stirring for 6 days. Purification yielded **PSAcGal$_{18}$** (690 mg, 57%). ^{1}H NMR (400 MHz, $CDCl_3$): δ_{ppm} 7.65 (br s, 1H), 7.15-6.15 (br, 4H), 5.37 (br s, 1H), 5.15(br, 1H), 4.98 (br s, 1H), 4.67-4.28(br, 7H), 4.23 (s, 1H), 4.12 (m, 2H), 3.92 (br s, 2H), 2.18-1.77 (m, 13H), 1.75-1.09 (br, 4H), 1.25 (m, 4H), 0.83 (br s, 1H). SEC: M_n = 10,000 g/mol, M_w = 11,000 g/mol, $Đ$ = 1.1.

Synthesis of PSGal$_8$ and the general procedure for the deprotection of PSAcGal. **PSAcGal$_8$** (350 mg, 75 μmol, 1.0 equiv.) was deposited in a flame dried round bottom flask and dissolved in 10 mL of anhydrous methanol. The reaction flask was placed in a 0 ºC ice bath and sodium methoxide (200 mg, 3.7 mmol, 50 equiv.) solid was added to the flask slowly. The flask was removed from the ice bath after 30 min and allowed to warm to room temperature. The reaction mixture was stirred for 16 h and checked by thin layer chromatography (TLC) (100% Methanol) to confirm complete deprotection. The pH of the resulting solution was adjusted to 7 using NH_4Cl and concentrated. The resulting crude compound was dissolved in 2 mL of DI water and purified by dialysis against DI water using a 2,000 MWCO membrane. The water was removed using a freeze dryer

affording **PSGal$_8$** (190 mg, 72%). ^{1}H NMR (400 MHz, D_2O): δ_{ppm} 7.91-7.32 (br), 7.10-5.83 (br), 4.25-2.91 (br), 2.89-2.62 (br), 1.55-1.37 (br), 1.24-1.05 (br), 0.84-0.20 (br).

Synthesis of PSGal$_{18}$. The polymer was deprotected by the same procedure described for **PAcGal$_8$** except for the following amounts were used. **PSAcGal$_{18}$** (500 mg, 50 μmol, 1.0 equiv.) and sodium methoxide (200 mg, 3.7 mmol, 74 equiv.). Purification yielded **PSGal$_{18}$** (230 mg, 63%). ^{1}H NMR (600 MHz, D_2O): δ_{ppm} 8.27-7.74 (br), 7.43-6.02 (br), 4.75-3.14 (br), 2.05-0.45 (br).

Synthesis of PSGal$_8$-Rho and the general procedure for the Rhodamine labelling PSGal. **PSGal$_8$** (150 mg, 48 μmol, 1.0 equiv.) was dissolved in minimal DMF. EDC·HCl (16 mg, 100 μmol 2.1 equiv.), DPTS (3.6 mg, 17 μmol, 0.35 equiv.), and DMAP (2 mg, 20 μmol, 0.4 equiv.) were added to the stirring solution simultaneously. Rhodamine B (3.2 mg, 6.7 μmol, 0.14 equiv.) was then added to the solution slowly. The solution was stirred overnight. The crude reaction mixture was dialyzed against 1L of DI water using 2,000 MWCO dialysis tubing for 48 h, with the dialysate being changed twice. The polymer solution was concentrated yielding **PSGal$_8$-Rho**. The polymer was used as-is and was not fully characterized. λ_{max} Absorbance = 510 nm. λ_{max} Emission = 584 nm. Extinction Coefficient = 618,000 mL/mg at 584 nm.

Synthesis of PSGal$_{18}$-Rho. The polymer was labelled by the same procedure described for **PAcGal$_8$-Rho** except for the following amounts were used. **PSGal$_{18}$** (100 mg, 10 μmol, 1.0 equiv.)**,** EDC·HCl (3.6 mg, 23 μmol, 2.3 equiv.), DPTS (0.82 mg, 3.8 μmol, 0.38 equiv.), DMAP (0.5 mg, 4 μmol, 0.40 equiv.), and Rhodamine B (3.2 mg, 1.5 μmol, 0.15 equiv.) The polymer solution was concentrated yielding **PSGal$_{18}$-Rhodamine**. The polymer was used as-is and was not fully characterized. λ_{max} Absorbance = 510 nm. λ_{max} Emission = 574 nm. Extinction Coefficient = 813,000 mL/mg at 574 nm.

Synthesis of MeO-PEG-N$_3$ (550) and the general procedure for the synthesis of PEG-N$_3$ compounds. Compound **10**[48] (20 g, 33 mmol, 1.0 equiv.) was dissolved in DMF. Sodium azide (21 g, 320 mmol, 9.7 equiv.) was added with stirring. An air condenser was added to the flask, which was then heated to 80 ºC and stirred overnight.

The DMF was removed *in vacuo* and the crude product was dissolved in 500 mL of dichloromethane, filtered, and then washed with DI water (30 mL x2). The organic phase was concentrated, then water was removed using a toluene wash (3 x 200 mL). The product was dissolved in minimal dichloromethane and precipitated into cold diethyl ether. The ether was decanted, the precipitate collected, and dried on high vacuum to yield **MeO-PEG-N_3 (550)** (14 g, 75%). ^{1}H NMR (400 MHz, $CDCl_3$): δ_{ppm} 3.68-3.62 (m, 49H), 3.56-3.52 (m, 2H), 3.40-3.35 (m, 5H). FT-IR: 2865, 2103, 1456, 1348, 1293, 1249, 1100 cm^{-1}. SEC: M_n = 380 g/mol, M_w = 490 g/mol, $Đ$ = 1.3.

Synthesis of N_3-PEG-N_3 (600). The azide was substituted by the same procedure described for **MeO-PEG-N_3 (550)** except for the following amounts were used. Compound **13**[48] (18 g, 25 mmol, 1.0 equiv.) and sodium azide (18 g, 280 mmol, 11 equiv.). Purification yielded **N_3-PEG-N_3 (600)** (14 g, 75%). ^{1}H NMR (400 MHz, $CDCl_3$): δ_{ppm} 3.66-3.59 (m, 57H), 3.36 (t, J = 12 Hz, 4H). FT-IR: 2865, 2098, 1456, 1347, 1287, 1249, 1100 cm^{-1}. SEC: M_n = 470 g/mol, M_w = 571 g/mol, $Đ$ = 1.2.

Synthesis of N_3-PEG-N_3 (1000). The azide was substituted by the same procedure described for **MeO-PEG-N_3 (550)** except for the following amounts were used. Compound **14**[48] (20 g, 20 mmol, 1.0 equiv.) and sodium azide (11 g, 170 mmol, 8.5 equiv.). Purification yielded **N_3-PEG-N_3 (1000)** (14 g, 75%). ^{1}H NMR (600 MHz, $CDCl_3$): δ_{ppm} 3.59-3.51 (m, 91H), 3.29 (t, J = 6 Hz, 4H). FT-IR: 2865, 2098, 1456, 1347, 1287, 1249, 1100 cm^{-1}. SEC: M_n = 1,400 g/mol, M_w = 1,500 g/mol, $Đ$ = 1.1.

Synthesis of MeO-PEG-PEtG$_{UV}$-PEG-OMe and the general procedure for the coupling of PEG to PEtG. **MeO-PEG-N_3 (550)** (30 mg, 52 µmol, 19 equiv.) was dissolved in 2 mL of DMF. 10 mg of $CuSO_4$, 10 mg of (+)-sodium L-ascorbate, and **PEtG$_{UV}$** (150 mg, 2.8 µmol, 1.0 equiv.) were subsequently added to the solution. The solution was heated with stirring for 18 h at 40 ºC. The resulting solution was dialyzed against 1L DI water, using a 3,500 g/mol MWCO membrane, overnight. The water was removed using a freeze dryer to yield **MeO-PEG-PEtG-PEG-OMe** (120 mg, 78%). ^{1}H NMR (400 MHz, $CDCl_3$): δ_{ppm} 5.70-5.52 (m, 833H), 4.21 (br s, 1705), 3.67-3.52 (br,

100H), 1.30-1.27 (m, 2591H). FT-IR: 2984, 2917, 2850, 1750, 1215, 1013, and 957cm^{-1}. SEC: M_n = 65,000 g/mol, M_w = 271,000 g/mol, $Đ$ = 4.2.

Synthesis of N_3-PEG-PEtG$_{UV}$-PEG-N_3 (600). **N_3-PEG-N_3 (600)** was coupled to **PEtG$_{UV}$** by the same procedure described for **MeO-PEG-PEtG$_{UV}$-PEG-OMe** except for the following amounts were used. **N_3-PEG-N_3 (600)** (120 mg, 190 μmol, 68 equiv.), 10 mg of $CuSO_4$, 10 mg of (+)-sodium L-ascorbate, and **PEtG$_{UV}$** (150 mg, 2.8 μmol, 1.0 equiv.). Purification yielded **N_3-PEG-PEtG$_{UV}$-PEG-N_3 (600)** (120 mg, 78%). ^{1}H NMR (600 MHz, $CDCl_3$): δ_{ppm} 5.73-5.46 (m, 868H), 4.22 (br s, 1757), 3.67-3.54 (br, 109H), 1.30-1.27 (m, 2788H). FT-IR: 2984, 2917, 2850, 1750, 1215, 1013, and 957cm^{-1}. SEC: M_n = 60,000 g/mol, M_w = 162,000 g/mol, $Đ$ = 2.7.

Synthesis of N_3-PEG-PEtG$_{UV}$-PEG-N_3 (1000). **N_3-PEG-N_3 (1000)** was coupled to **PEtG$_{UV}$** by the same procedure described for **MeO-PEG-PEtG$_{UV}$-PEG-OMe** except for the following amounts were used. **N_3-PEG-N_3 (1000)** (300 mg, 270 μmol, 96 equiv.), 10 mg of $CuSO_4$, 10 mg of (+)-sodium L-ascorbate, and **PEtG$_{UV}$** (150 mg, 2.8 μmol, 1.0 equiv.). Purification yielded **N_3-PEG-PEtG$_{UV}$-PEG-N_3 (1000)** (120 mg, 78%). ^{1}H NMR (600 MHz, $CDCl_3$): δ_{ppm} 5.71-5.46 (m, 965H), 4.22 (br s, 1952H), 3.66-3.56 (br, 184H), 1.30-1.27 (m, 3028H). FT-IR: 2984, 2917, 2850, 1750, 1215, 1013, and 957cm^{-1}. SEC: M_n = 108,000 g/mol, M_w = 492,000 g/mol, $Đ$ = 4.6.

PBD-PEG Nanoparticle Preparation. The procedure was adapted from a previously reported method.[42] In a 3-mL dram vial, 5.0 mg of polymer (**PBD-PEG-OH**, **PBD-PEG-N_3,** or a mixture) was mixed with 50 μg of the hydrophobic dye Nile Red in 0.5 mL of chloroform and then the solvent was evaporated under a stream of nitrogen gas. The resulting thin film was further dried under high vacuum overnight to remove traces of solvent. The thin film was then hydrated overnight with 0.5 mL of filtered Ultrapure water and kept at 46 °C. A stir bar was then added to the vial and it was rapidly stirred (1000 rpm or greater) overnight. The vesicles were then imaged by confocal laser scanning microscopy (see below).

PEG-PEtG-PEG Nanoparticle Preparation. 8 μL of 0.1 mg/mL perylene in dichloromethane solution was added to a dram vial and the solvent was evaporated using

a stream of nitrogen gas. 100 μL of 8 mg/mL triblock in THF (**MeO-PEG-PEtG-PEG-OMe** or **N_3-PEG-PEtG-PEG-N_3**, or a mixture of both) triblock in THF was added to the vial along with a small magnetic stir bar. The solution was stirred for 5 min, then at a stir rate of 400 rpm, 0.9 mL of DI water was added dropwise (~1 drop per second). After stirring for another 20 min, the suspension was transferred to a 50,000 MWCO dialysis membrane and dialyzed against 1L of DI water to remove the THF. The resulting suspension was stored in a 4 ºC fridge.

Confocal Laser Scanning Microscopy (CLSM). 10 μL of the aqueous suspension of polymersomes was dropped onto a glass slide, a glass coverslip was placed on top, and the outside edges of the coverslip were sealed with nail polish. The slides were stored at 4 ºC for 2 h prior to imaging. Images were obtained using a confocal laser scanning microscope (LSM 510, Carl Zeiss Inc.) using a 63X (Nanoparticles suspensions which contained Nile Red) and 100X (Nanoparticles suspensions which contained **PAGal-Rhodamine**, **PSGal-Rhodamine**, or perylene) oil immersion objective, and an excitation wavelength of 543 nm (Nanoparticles suspensions which contained Nile Red, **PAGal-Rhodamine**, or **PSGal-Rhodamine**) and 405 nm (Nanoparticles suspensions which contained perylene).

Fluorescence Calibration Curves. **PAGal-Rhodamine** and **PSGal-Rhodamine** were dissolved in dimethyl sulfoxide (DMSO) to achieve a concentration of 0.25 mg/mL. The solution was then diluted with DMSO to obtain measurements at a minimum of four different concentrations ranging from 0.05 mg/mL to 0.25 mg/mL. Acquisition settings were as follows: Excitation @ 562 nm, Emission from 565 to 610 nm, Length = 45 nm, Step Size = 0.25 nm, Integration = 1 s, Averages = 1. The 3 mL glass cuvette was rinsed 3 times with 1.5 mL of DMSO between samples. All measurements were taken in triplicate and then averaged to obtain the values used for the calibration curve.

Fluorescence Spectroscopy to Quantify Azide-Alkyne Click. Each nanoparticle suspension had the water removed using a freeze dryer to yield a powdered sample. The sample was then dissolved in 1 mL of DMSO. The fluorescence counts were then measured using the same parameters used to create the calibration curves. All

measurements were taken in triplicate and then averaged to obtain the concentration values.

Method to Calculate the Percentage of Functionalized Azide Groups. To calculate the percentage of functionalized N_3 groups, first the theoretical yield of the click reaction was determined. The mass of the **PBD-PEG** was adjusted for the relative amount of azide density, where polymer samples containing 10% **PBD-PEG-N_3** were multiplied by 0.1 and 100% azide functionalized **PBD-PEG-N_3** were multiplied by 1. The mass was then adjusted for the amount of available azide due to the nature of vesicles. **PBD-PEG-N_3** will be on the inside of the polymersome, with the expected ratio being 50:50 inside: outside. To make the appropriate adjustment, the mass was multiplied by 0.5. The moles of azide were calculated by dividing the mass of available azide by the molar mass of the **PBD-PEG-N_3** which was approximately 10000 g/mol. The moles of azide were assumed to be equal to the moles of alkyne functionalized glycopolymer as they react in a 1:1 ratio. Multipling the moles of alkyne functionalized glycopolymer by the molar mass of the respective polymer, short glycopolymer = 2,400 g/mol or long glycopolymer = 5,200 g/mol, the expected or theoretical mass of dyed glycopolymer was determined. The experimental yield or mass of dyed glycopolymer, determined using the calibration curve, was divided by the theoretical yield to determine the percent functionalization of the azide groups on the vesicles.

Chapter 4

4 Conclusions and Future Work

The work in this thesis provided progress towards producing glycopolymer functionalized polymersomes and quantifying their degree of functionalization. It was shown that the degree of **PBD-PEG** polymersome surface functionalization could be quantified by measuring the fluorescence of a glycopolymer, **PAGal**, labelled with rhodamine B. Difficulty with the synthesis of the **PAAcGal** led to the development and synthesis of a second glycopolymer with pendent β-D-galactose moieties, **PSAcGal**. **PSAcGal** having two different DP_n values were synthesized, deprotected, and labelled with rhodamine B.

The shorter dye-labelled glycopolymer was conjugated to the surface of **PBD-PEG** polymersomes, yielding similar surface functionalization as the previous glycopolymer, **PAGal**. The relative amount of functionalization that could be achieved when the polymersomes had 10% compared to 100% of the surface containing an azide group, was determined for each length of dye-labelled glycopolymer. The results indicated that the length of the glycopolymer did not significantly affect the yield of the CuAAC reaction, but that a higher yield was obtained at lower azide densities. It is speculated that the high degree of steric hindrance associated with functionalizing every azide group on the surface of the polymersome decreased CuAAC reaction yields for 100% azide coated polymersomes.

Although initial conjugation experiments were performed, there were subsequently issues with the reproducibility of the **PBD-PEG** polymersomes. The issues of reproducibility lead to the proposal of an alternative block copolymer platform. A triblock polymer, **MeO-PEG-PEtG$_{UV}$-PEG-OMe**, previously shown to reproducibly form polymersomes, that could be functionalized with azide groups. A new **MeO-PEG-PEtG$_{UV}$-PEG-OMe (550)** triblock and two azide functionalized triblock polymers, **N$_3$-PEG-PEtG$_{UV}$-PEG-N$_3$ (600)** and **PEG-PEtG$_{UV}$-PEG-N$_3$ (1000)**, were produced and characterized. The self-

assembly of **MeO-PEG-PEtG$_{UV}$-PEG-OMe** and **N$_3$-PEG-PEtG$_{UV}$-PEG-N$_3$** triblock polymers individually and in mixtures led to the formation of nanoparticles that were too small to be imaged by CLSM. However, the mixture of a thermo-responsive analog triblock, **MeO-PEG-PEtG$_{Thermo}$-PEG-OMe**, and **N$_3$-PEG-PEtG$_{UV}$-PEG-N$_3$** yielded suspensions containing large polymersomes that could be imaged with CLSM along with smaller particles. CLSM could not be used to determine if the smaller particles were polymersomes or not.

In terms of future work, the self-assembly protocol of **MeO-PEG-PEtG$_{Thermo}$-PEG-OMe** and **N$_3$-PEG-PEtG$_{UV}$-PEG-N$_3$** mixtures must be optimized to achieve monodisperse samples of large polymersomes. These large polymersomes could then be functionalized with dye-labelled glycopolymers to determine the relative functionalization densities. The binding of the glycopolymer functionalized polymersomes could then be determined with lectin binding assays. Alternatively, if the small nanoparticles produced by **N$_3$-PEG-PEtG$_{UV}$-PEG-N$_3$** can be imaged with TEM and a vesicle morphology is observed, then they would be another candidate for further functionalization with glycopolymers. The next steps towards optimizing a PEtG containing triblock that can be self-assembled into polymersomes and functionalized with glycopolymers involves synthesizing triblock polymers with lower dispersities. Triblock polymers with lower dispersities would likely increase the reproducibility of polymersome formation by making the hydrophilic weight fraction more consistent within a polymer sample. Since hydrophilic weight fraction affects the morphology achieved with self-assembly, lower dispersities should make the self-assembly results more consistent. Reproducibly producing functionalizable polymersomes would create opportunities to take advantage of the tuneable degradation of the PEtG block. A system can be imagined where glycopolymers on the outside of a polymersome allow for specific targeting of a pathogen. After binding the pathogen, an enzyme, change in pH, or the presence of reducing agents at the surface of the pathogen could cause the degradation of the polymersome, releasing an anti-viral or anti-bacterial drug.

References

(1) Hakomori, S.; Igarashi, Y. Functional-Role Of Glycosphingolipids In Cell Recognition And Signaling. *J. Biochem.* **1995**, *118*, 1091–1103.

(2) Mrksich, M. A Surface Chemistry Approach to Studying Cell Adhesion. *Chem. Soc. Rev.* **2000**, *29*, 267–273.

(3) Jones, F. S.; Jones, P. L. The Tenascin Family of ECM Glycoproteins : Structure , Function , and Regulation During Embryonic Development and Tissue Remodeling. *Pediatr. Res.* **2000**, *259*, 235–259.

(4) Lis, H.; Sharon, N. Lectins: Carbohydrate-Specific Proteins That Mediate Cellular Recognition. *Chem. Rev.* **1998**, *98*, 637–674.

(5) Wang, B.; Boons, G.-J. *Carbohydrate Recognition- Biological Problems, Methods and Applications*; John Wiley & Sons, Inc.: Hoboken, **2011**.

(6) Turner, M. W. The Role of Mannose-Binding Lectin in Health and Disease. *Neth. J. Med.* **2004**, *62*, 4–9.

(7) Nazemi, A.; Haeryfar, S. M. M.; Gillies, E. R. Multifunctional Dendritic Sialopolymersomes as Potential Antiviral Agents: Their Lectin Binding and Drug Release Properties. *Langmuir* **2013**, *29*, 6420–6428.

(8) Medzhitov, R.; Janeway Jr., C. A. Decoding the Pattern of Self and Nonself by the Innate Immune System. *Science.* **2002**, *296*, 298–300.

(9) Schauer, R. Sialic Acids and Their Role as Biological Masks. *Trends Biochem. Sci.* **1985**, *10*, 357–360.

(10) Guo, Z.; Boons, G. *Carbohydrate-Based Vaccines and Immunotherapies*; John Wiley & Sons, Inc.: Hoboken, **2009**.

(11) Houghton, B. A. N. Cancer Antigens : Immune Recognition of Self and Altered

Self. *J. Exp. Med.* **1994**, *180*, 1–4.

(12) Quiocho, F. A. Carbohydrate-Binding Proteins: Tertiary Structures and Protein-Sugar Interactions. *Annu. Rev. Biochem.* **1986**, *55*, 287–315.

(13) Sharon, N.; Lis, H. *Lectins*, 2nd ed.; Kluwer Academic Publishers: Dordrecht, **2003**.

(14) Weis, W. I.; Drickamer, K. Structural Basis for Lectin-Carbohydrate Recognition. *Annu. Rev. Biochem.* **1996**, *65,* 471-473.

(15) Clarke, C.; Woods, R. J.; Gluska, J.; Cooper, A.; Nutley, M. A.; Boons, G. Involvement of Water in Carbohydrate - Protein Binding. *J. Am. Chem. Soc.* **2001**, *16*, 12238–12247.

(16) Muzzarelli, R. A. A.; Greco, F.; Busilacchi, A.; Sollazzo, V.; Gigante, A. Chitosan, Hyaluronan and Chondroitin Sulfate in Tissue Engineering for Cartilage Regeneration: A Review. *Carbohydr. Polym.* **2012**, *89*, 723–739.

(17) Garg, H. G.; Cowman, M. K.; Hales, C. A. *Carbohydrate Chemistry, Biology and Medical Applications*, 1st ed.; Elsevier Ltd: Amsderdam, **2008**.

(18) Lee, C. C.; MacKay, J. A.; Fréchet, J. M. J.; Szoka, F. C. Designing Dendrimers for Biological Applications. *Nat. Biotechnol.* **2005**, *23*, 1517–1526.

(19) Mammen, M.; Choi, S. K.; Whitesides, G. M. Polyvalent Interactions in Biological Systems: Implications for Design and Use of Multivalent Ligands and Inhibitors. *Angew. Chemie - Int. Ed.* **1998**, *37*, 2754–2794.

(20) Tsuchida, A.; Kobayashi, K.; Matsubara, N.; Muramatsu, T.; Suzuki, T.; Suzuki, Y. Simple Synthesis of Sialyllactose-Carrying Polystyrene and Its Binding with Influenza Virus. *Glycoconj. J.* **1998**, *15*, 1047–1054.

(21) Ohta, T.; Miura, N.; Fujitani, N.; Nakajima, F.; Niikura, K.; Sadamoto, R.; Guo, C. T.; Suzuki, T.; Suzuki, Y.; Monde, K.; et al. Glycotentacles: Synthesis of Cyclic

Glycopeptides, Toward a Tailored Blocker of Influenza Virus Hemagglutinin. *Angew. Chemie Int. Ed.* **2003**, *42*, 5186–5189.

(22) Davis, B. G. Synthesis of Glycoproteins. *Chem. Rev.* **2002**, *102*, 579–601.

(23) Pratt, M. R.; Bertozzi, C. R. Synthetic Glycopeptides and Glycoproteins as Tools for Biology. *Chem. Soc. Rev.* **2005**, *34*, 58.

(24) Hölemann, A.; Seeberger, P. H. Carbohydrate Diversity: Synthesis of Glycoconjugates and Complex Carbohydrates. *Curr. Opin. Biotechnol.* **2004**, *15*, 615–622.

(25) Hu, Q.-Y.; Allan, M.; Adamo, R.; Quinn, D.; Zhai, H.; Wu, G.; Clark, K.; Zhou, J.; Ortiz, S.; Wang, B.; et al. Synthesis of a Well-Defined Glycoconjugate Vaccine by a Tyrosine-Selective Conjugation Strategy. *Chem. Sci.* **2013**, *4*, 3827.

(26) Turnbull, W. B.; Stoddart, J. F. Design and Synthesis of Glycodendrimers. *Rev. Mol. Biotechnol.* **2002**, *90*, 231–255.

(27) Trant, J. F.; Jain, N.; Mazzuca, D. M.; McIntosh, J. T.; Fan, B.; Haeryfar, S. M. M.; Lecommandoux, S.; Gillies, E. R. Synthesis, Self-Assembly, and Immunological Activity of α-Galactose-Functionalized Dendron–lipid Amphiphiles. *Nanoscale* **2016**, *8*, 17694–17704.

(28) André, S.; Cejas Ortega, P. J.; Ferez, M. A.; Roy, R.; Gabius, H. J. Lactose-Containing Starburst Dendrimers: Influence of Dendrimer Generation and Binding-Site Orientation of Receptors (Plant/animal Lectins and Immunoglobulins) on Binding Properties. *Glycobiology* **1999**, *9*, 1253–1261.

(29) Marradi, M.; Chiodo, F.; García, I.; Penadés, S. Glyconanoparticles as Multifunctional and Multimodal Carbohydrate Systems. *Chem. Soc. Rev.* **2013**, *42*, 4728.

(30) Barrientos, A. G.; de la Fuente, J. M.; Jiménez, M.; Solís, D.; Cañada, F. J.; Martín-Lomas, M.; Penadés, S. Modulating Glycosidase Degradation and Lectin

Recognition of Gold Glyconanoparticles. *Carbohydr. Res.* **2009**, *344*, 1474–1478.

(31) de la Fuente, J. M.; Barrientos, A. G.; Rojas, T. C.; Rojo, J.; Cañada, J.; Fernández, A.; Penadés, S. Gold Glyconanoparticles as Water-Soluble Polyvalent Models To Study Carbohydrate Interactions. *Angew. Chemie Int. Ed.* **2001**, *40*, 2257–2261.

(32) García, I.; Marradi, M.; Penadés, S. Glyconanoparticles: Multifunctional Nanomaterials for Biomedical Applications. *Nanomedicine.* **2010**, *5*, 777–792.

(33) Ahmed, M.; Deng, Z.; Liu, S.; Lafrenie, R.; Kumar, A.; Narain, R. Cationic Glyconanoparticles: Their Complexation with DNA, Cellular Uptake, and Transfection Efficiencies. *Bioconjug. Chem.* **2009**, *20*, 2169–2176.

(34) van Rijn, P.; Tutus, M.; Kathrein, C.; Zhu, L.; Wessling, M.; Schwaneberg, U.; Böker, A. Challenges and Advances in the Field of Self-Assembled Membranes. *Chem. Soc. Rev.* **2013**, *42*, 6578.

(35) Suriano, F.; Pratt, R.; Tan, J. P. K.; Wiradharma, N.; Nelson, A.; Yang, Y. Y.; Dubois, P.; Hedrick, J. L. Synthesis of a Family of Amphiphilic Glycopolymers via Controlled Ring-Opening Polymerization of Functionalized Cyclic Carbonates and Their Application in Drug Delivery. *Biomaterials* **2010**, *31*, 2637–2645.

(36) Ladmiral, V.; Semsarilar, M.; Canton, I.; Armes, S. P. Polymerization-Induced Self-Assembly of Galactose-Functionalized Biocompatible Diblock Copolymers for Intracellular Delivery. *J. Am. Chem. Soc.* **2013**, *135*, 13574–13581.

(37) Percec, V.; Leowanawat, P.; Sun, H. J.; Kulikov, O.; Nusbaum, C. D.; Tran, T. M.; Bertin, A.; Wilson, D. A.; Peterca, M.; Zhang, S.; et al. Modular Synthesis of Amphiphilic Janus Glycodendrimers and Their Self-Assembly into Glycodendrimersomes and Other Complex Architectures with Bioactivity to Biomedically Relevant Lectins. *J. Am. Chem. Soc.* **2013**, *135*, 9055–9077.

(38) Sherman, S. E.; Xiao, Q.; Percec, V. Mimicking Complex Biological Membranes and Their Programmable Glycan Ligands with Dendrimersomes and

Glycodendrimersomes. *Chem. Rev.* **2017**, *117*, 6538–6631.

(39) Martin, A. L.; Li, B.; Gillies, E. R. Surface Functionalization of Nanomaterials with Dendritic Groups : Toward Enhanced Binding to Biological Targets Surface Functionalization of Nanomaterials with Dendritic Groups : Toward Enhanced Binding to Biological Targets. *J. Am. Chem. Soc.* **2009**, *16*, 734–741.

(40) Chiefari, J.; Chong, Y. K.; Ercole, F.; Krstina, J.; Jeffery, J.; Le, T. P. T.; Mayadunne, R. T. A.; Meijs, G. F.; Moad, C. L.; Moad, G.; et al. Living Free-Radical Polymerization by Reversible Addition - Fragmentation Chain Transfer: The RAFT Process. *Macromolecules* **1998**, *31*, 5559–5562.

(41) York, A. W.; Kirkland, S. E.; McCormick, C. L. Advances in the Synthesis of Amphiphilic Block Copolymers via RAFT Polymerization: Stimuli-Responsive Drug and Gene Delivery. *Adv. Drug Deliv. Rev.* **2008**, *60*, 1018–1036.

(42) Li, B.; Martin, A. L.; Gillies, E. R. Multivalent Polymer Vesicles via Surface Functionalization. *Chem. Commun.* **2007**, *3*, 5217–5219.

(43) Nazemi, A.; Amos, R. C.; Bonduelle, C. V.; Gillies, E. R. Dendritic Surface Functionalization of Biodegradable Polymer Assemblies. *J. Polym. Sci. Part A Polym. Chem.* **2011**, *49*, 2546–2559.

(44) Raycraft, B. M. "Nanocarriers for Drug Delivery Applications : From Tunable Morphologies to Glycopolymer-Coated Vesicles" (2016).*Electronic Thesis and Dissertation Repository*. 4040. https://ir.lib.uwo.ca/etd/4040

(45) Fan, B.; Trant, J. F.; Hemery, G.; Sandre, O.; Gillies, E. R. Thermo-Responsive Self-Immolative Nanoassemblies: Direct and Indirect Triggering. *Chem. Commun.* **2017**, *53*, 12068–12071.

(46) Yu, K.; Kizhakkedathu, J. N. Synthesis of Functional Polymer Brushes Containing Carbohydrate Residues in the Pyranose Form and Their Specific and Nonspecific Interactions with Proteins. *Biomacromolecules* **2010**, *11*, 3073–3085.

(47) Ten Brummelhuis, N.; Weck, M. Orthogonal Multifunctionalization of Random and Alternating Copolymers. *ACS Macro Lett.* **2012**, *1*, 1216–1218.

(48) Nguyen, P. K.; Snyder, C. G.; Shields, J. D.; Smith, A. W.; Elbert, D. L. Clickable Poly (Ethylene Glycol) -Microsphere- Based Cell Scaffolds. *Macromol. Chem. Phys.* **2013**, *214,* 948–956.

Appendices

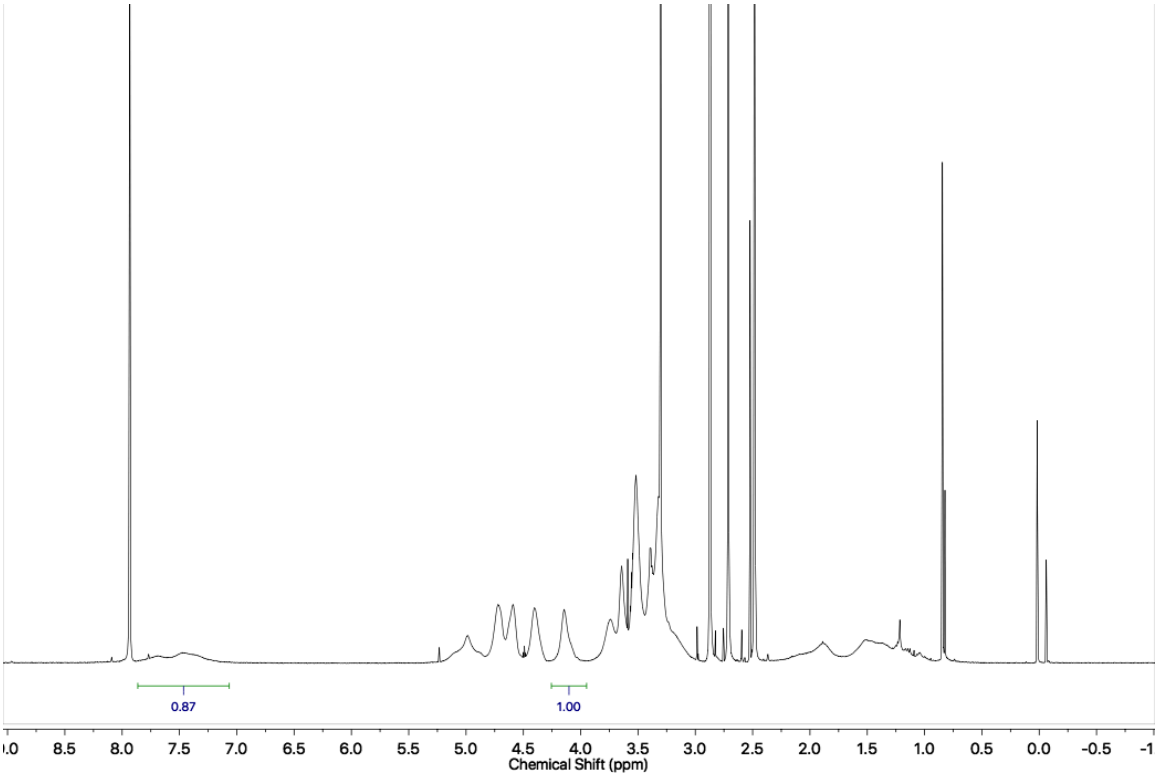

Figure A.0.1. ^{1}H NMR Spectrum of **PAGal$_{19}$-Rho.** (DMSO-d6, 400 MHz)

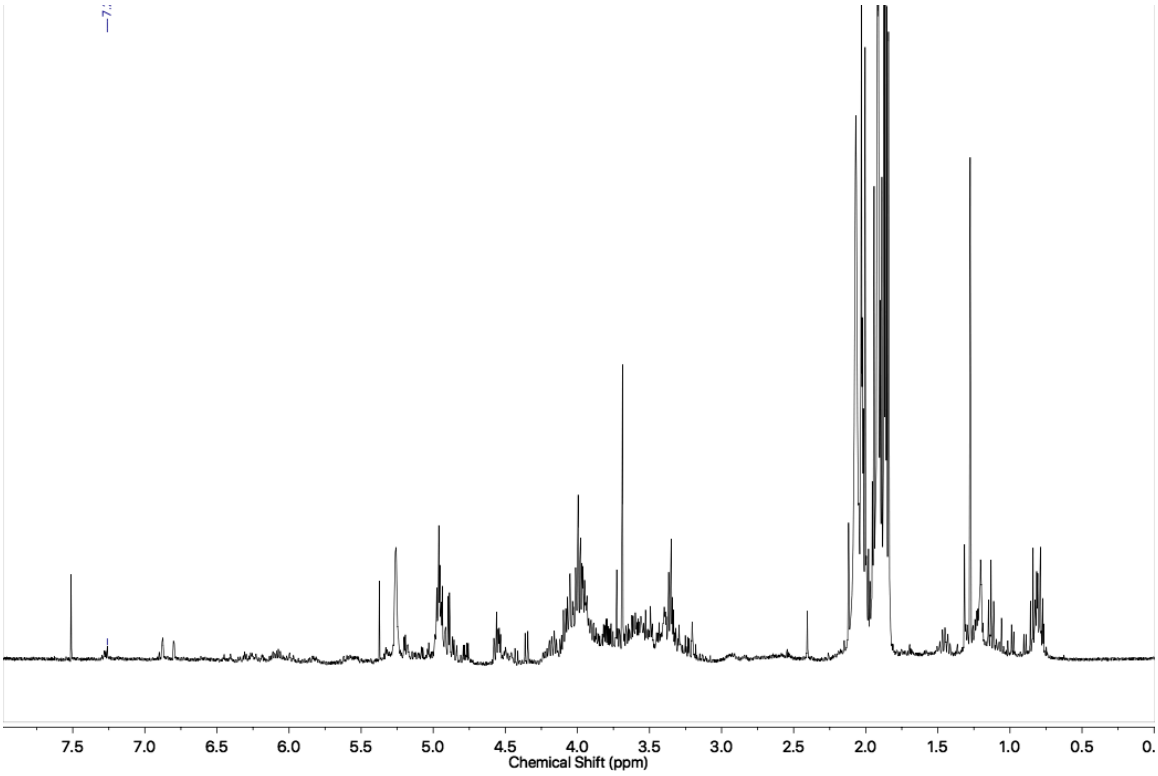

Figure A.0.2. ^{1}H NMR Spectrum of crude **AAcGal**. ($CDCl_3$, 600 MHz)

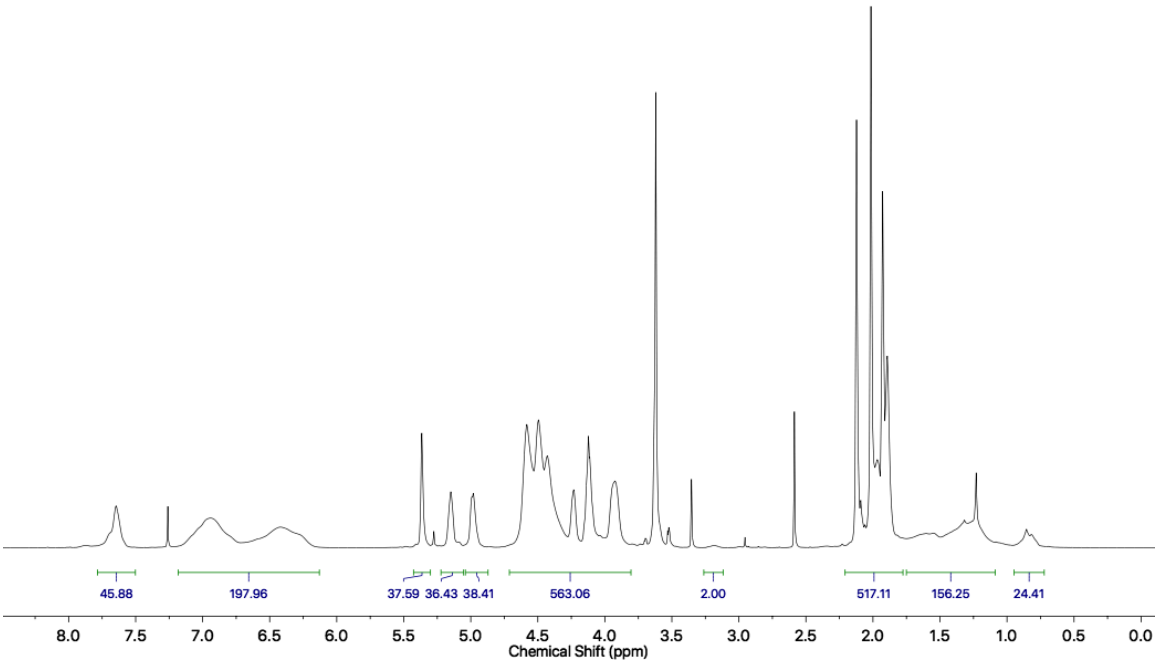

Figure A.0.3. ^{1}H NMR Spectrum of **PSAcGal$_{18}$**. ($CDCl_3$, 600 MHz)

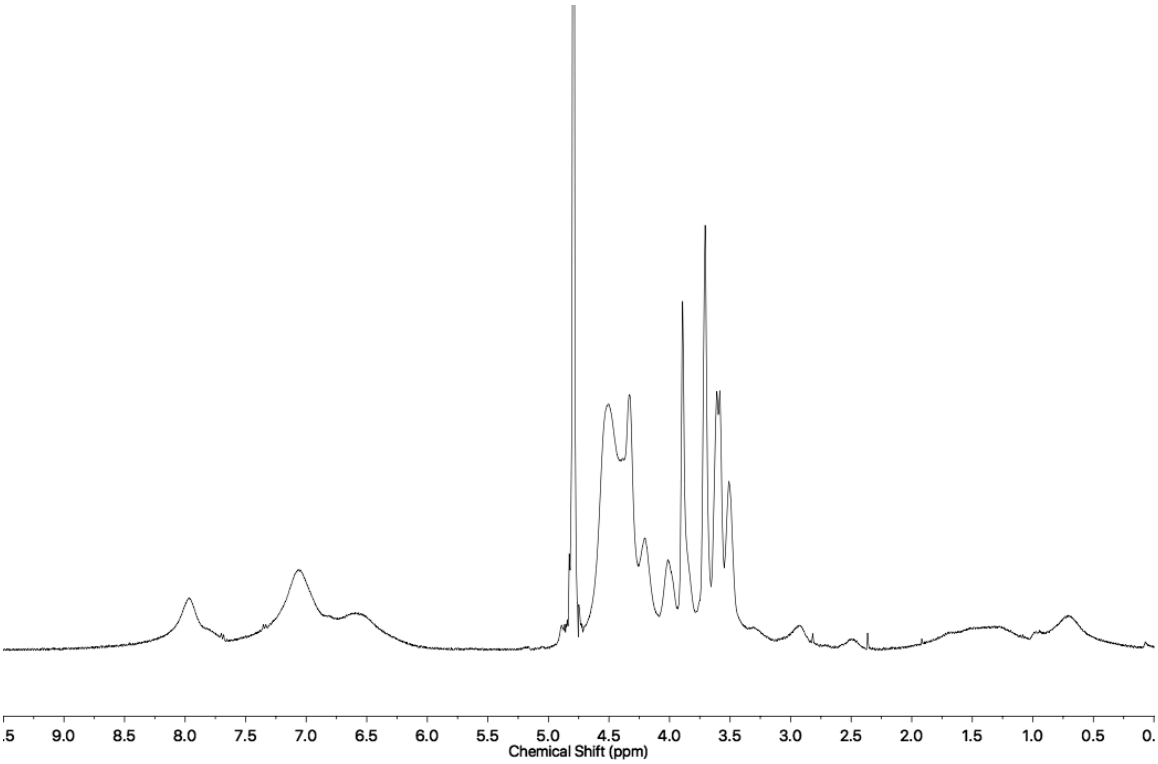

Figure A.0.4. ^{1}H NMR Spectrum of **PSGal$_8$-Rho**. (D_2O, 600 MHz)

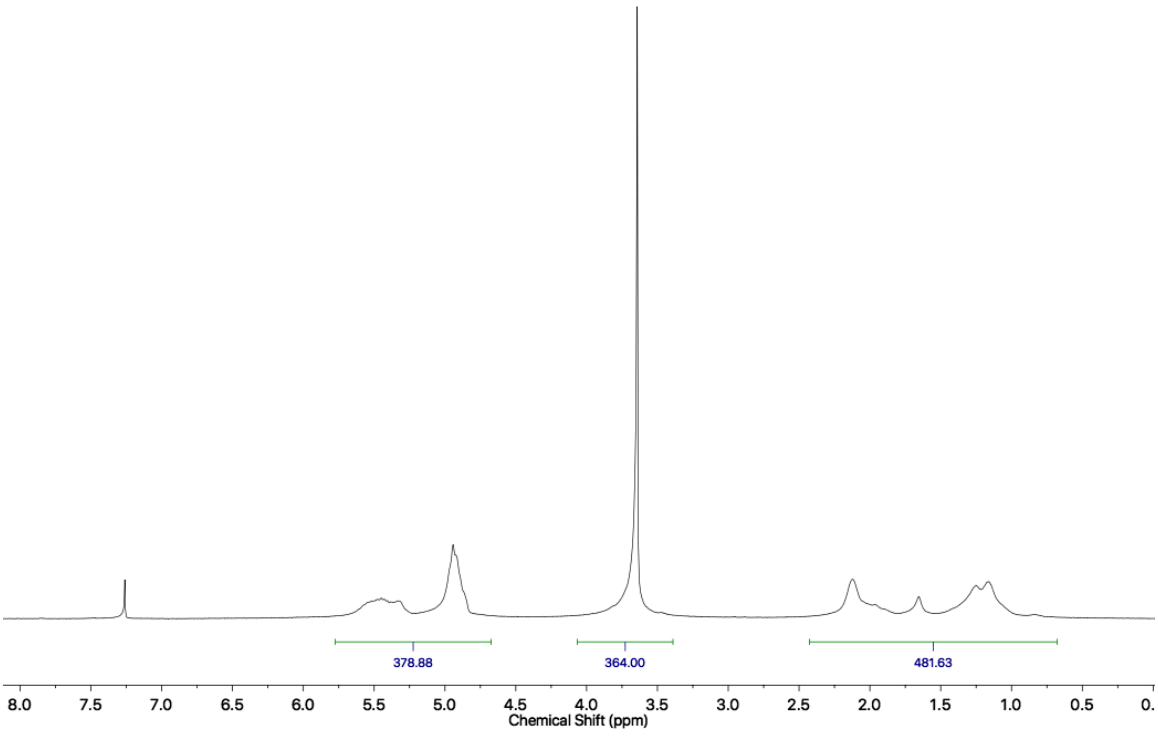

Figure A.0.5. ^{1}H NMR spectrum of **PBD-PEG-OH.** ($CDCl_3$, 400 MHz)

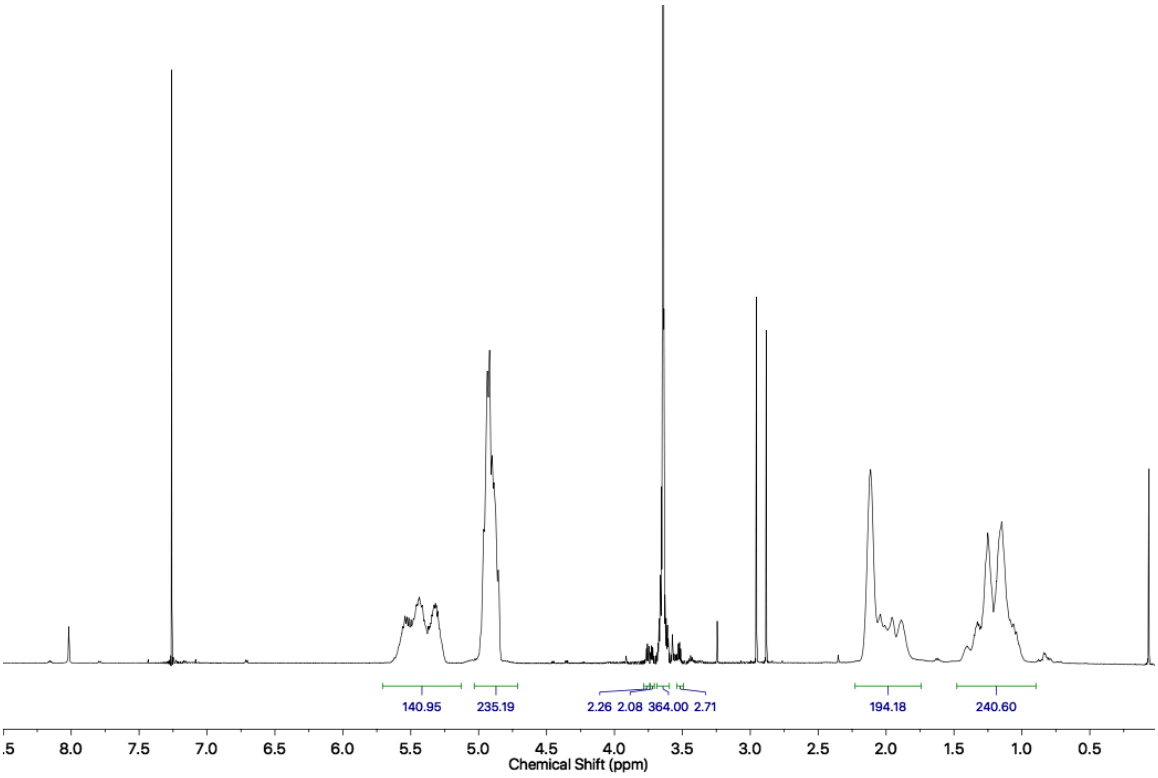

Figure A.0.6. ^{1}H NMR spectrum of **PBD-PEG-N$_3$**. ($CDCl_3$, 600 MHz)

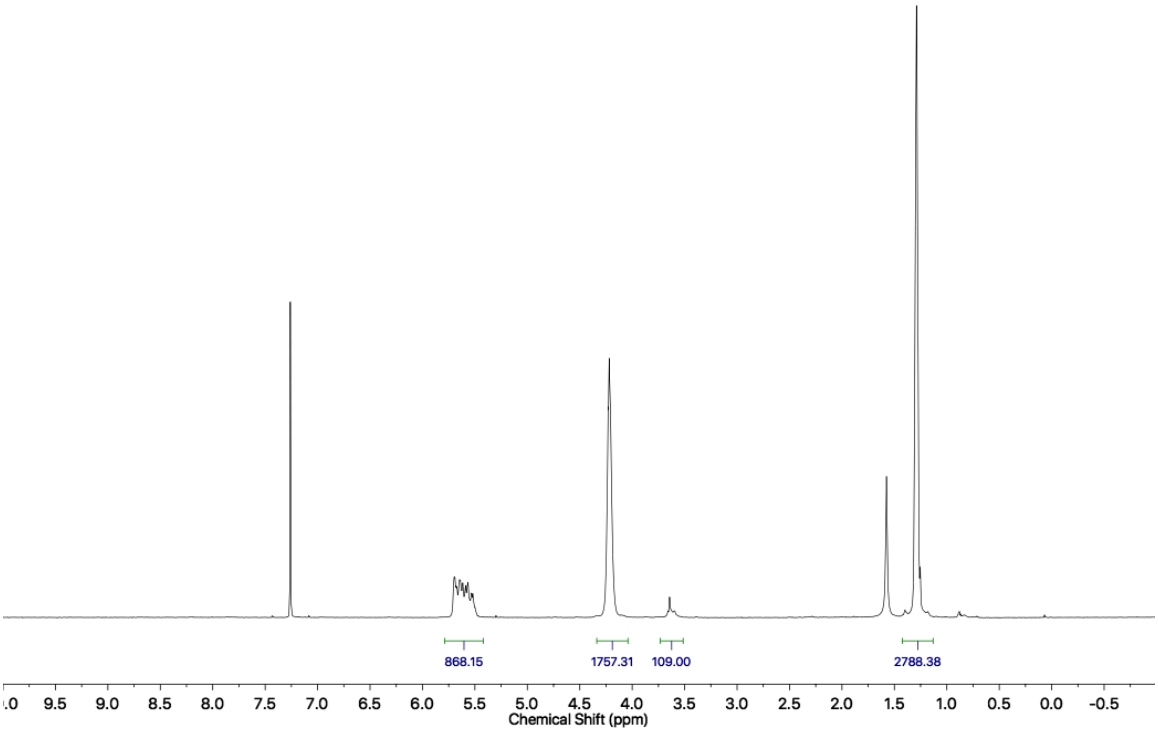

Figure A.0.7. ^{1}H NMR spectrum of **N$_3$-PEG-PEtG$_{UV}$-PEG-N$_3$ (600)**.($CDCl_3$, 600 MHz)

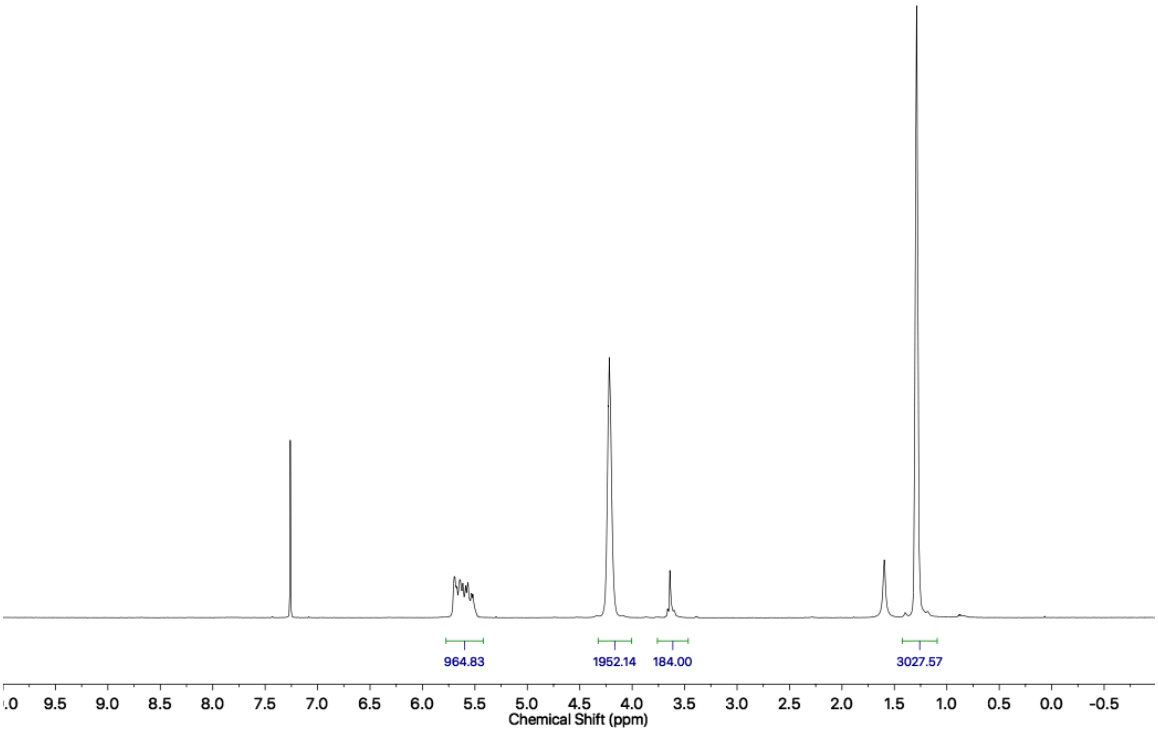

Figure A.0.8. ^{1}H NMR spectrum of **N_3-PEG-PEtG$_{UV}$-PEG-N_3 (1000)**. ($CDCl_3$, 600 MHz)

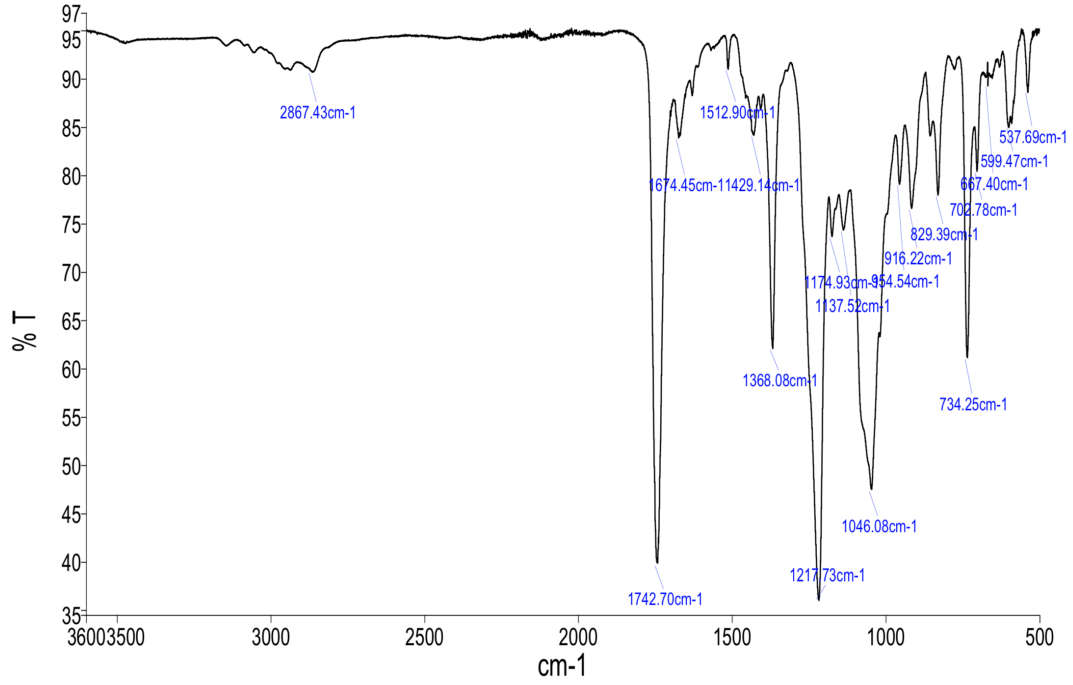

Figure A.0.9. FT-IR spectrum of **SAcGal**.

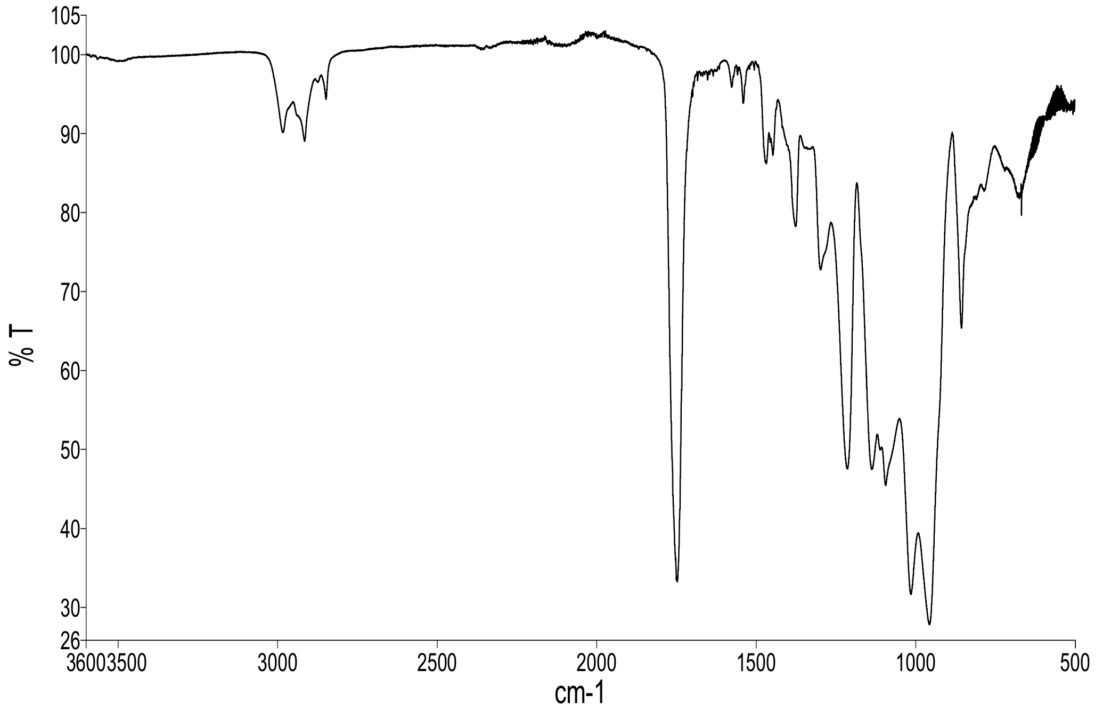

Figure A.0.10. FT-IR spectrum of **N_3-PEG-PEtG-PEG-N_3 (1000)**.

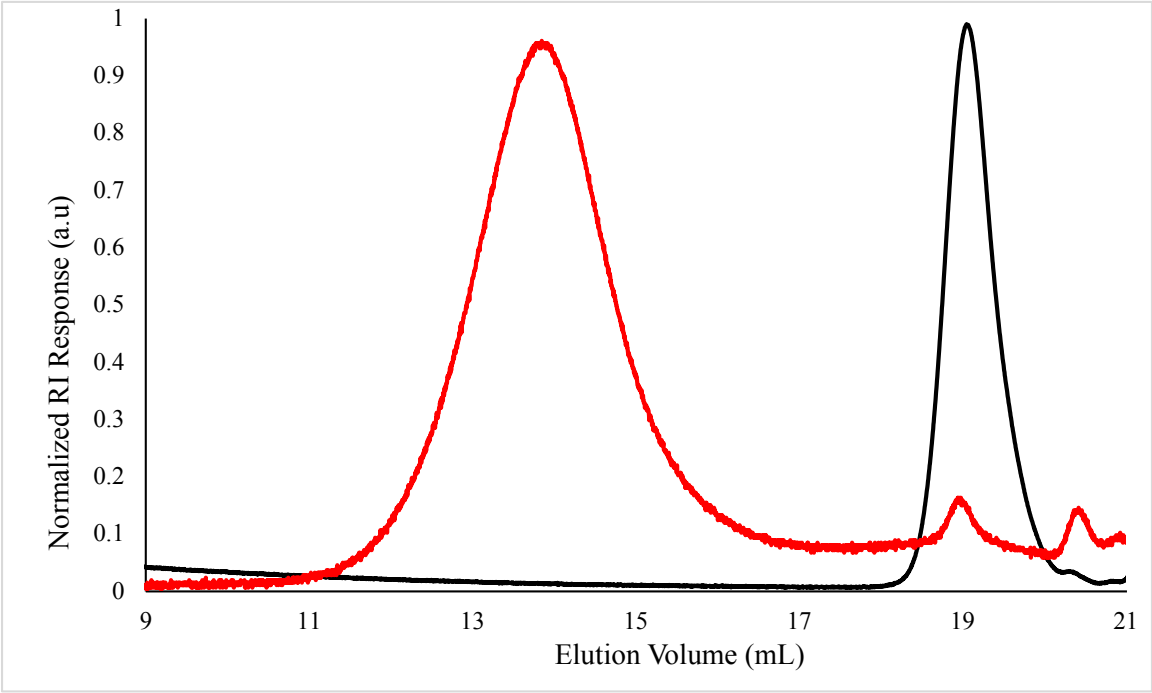

Figure A.0.11. SEC overlay of **N_3-PEG-PEtG-PEG-N_3 (600)** and **N_3-PEG-N_3 (600).**

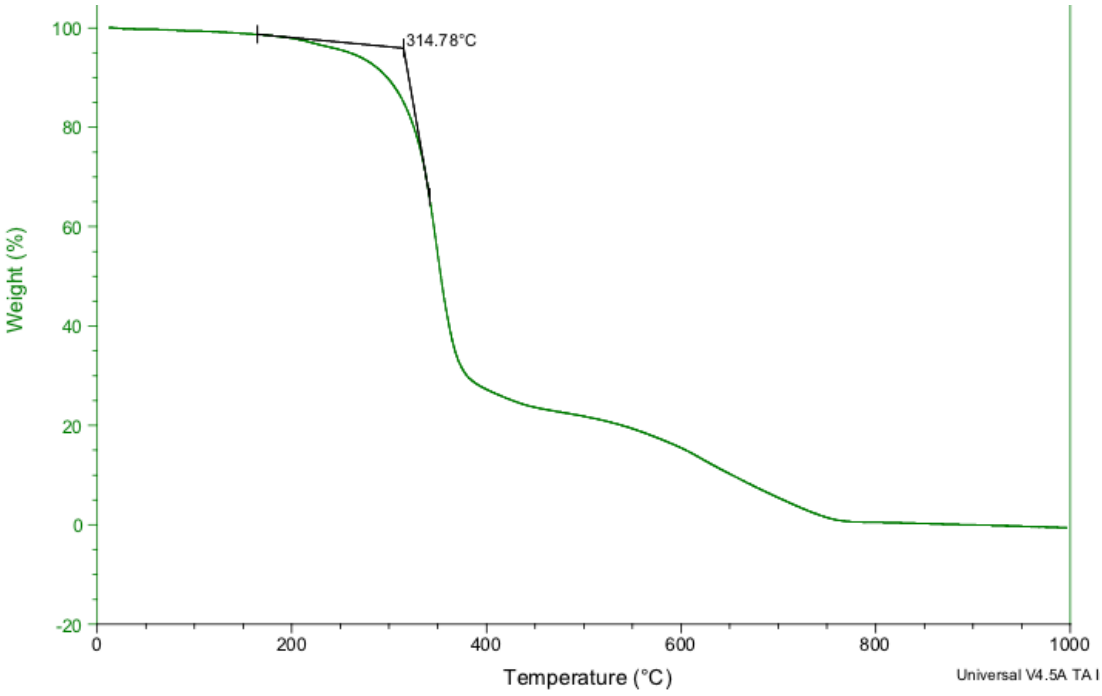

Figure A.0.12. TGA trace of **PSAcGal$_8$**.

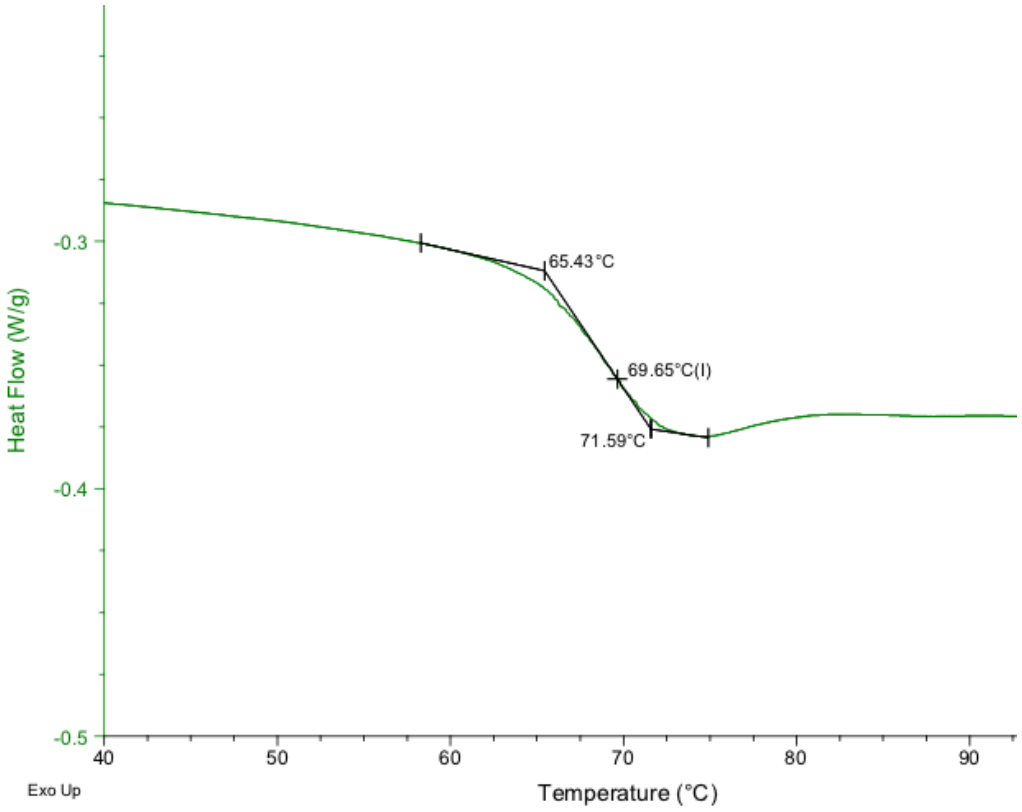

Figure A.0.13. DSC trace for **PSAcGal$_8$**.

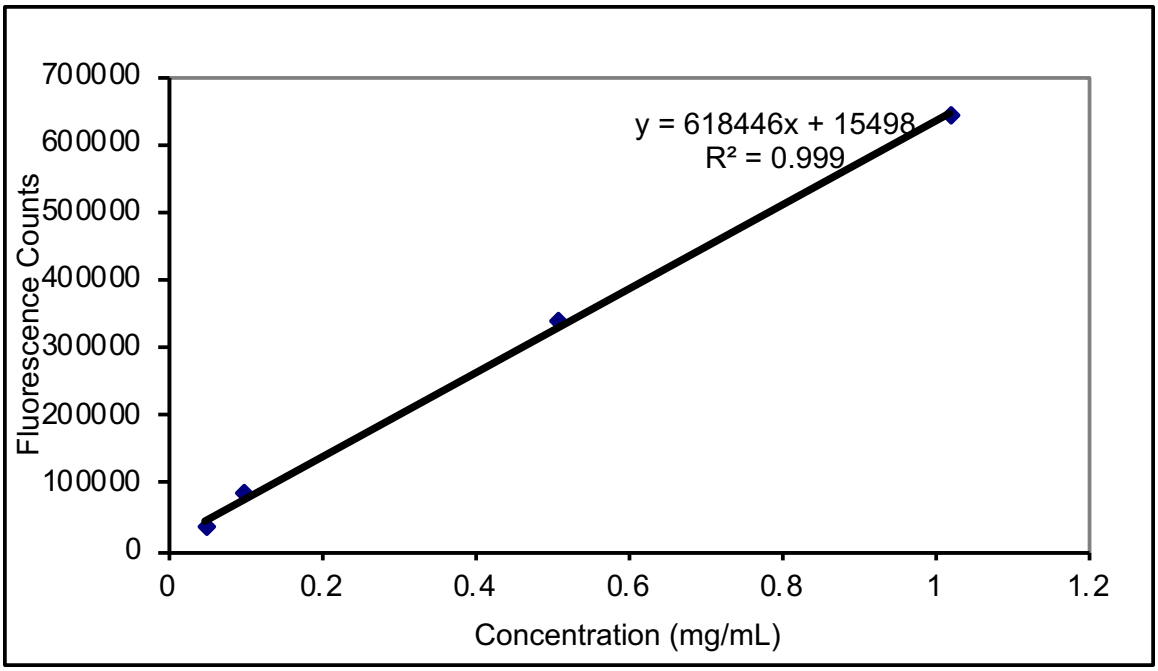

Figure A.0.14. Fluorescence Calibration Curve for **PSGal$_8$-Rho**.

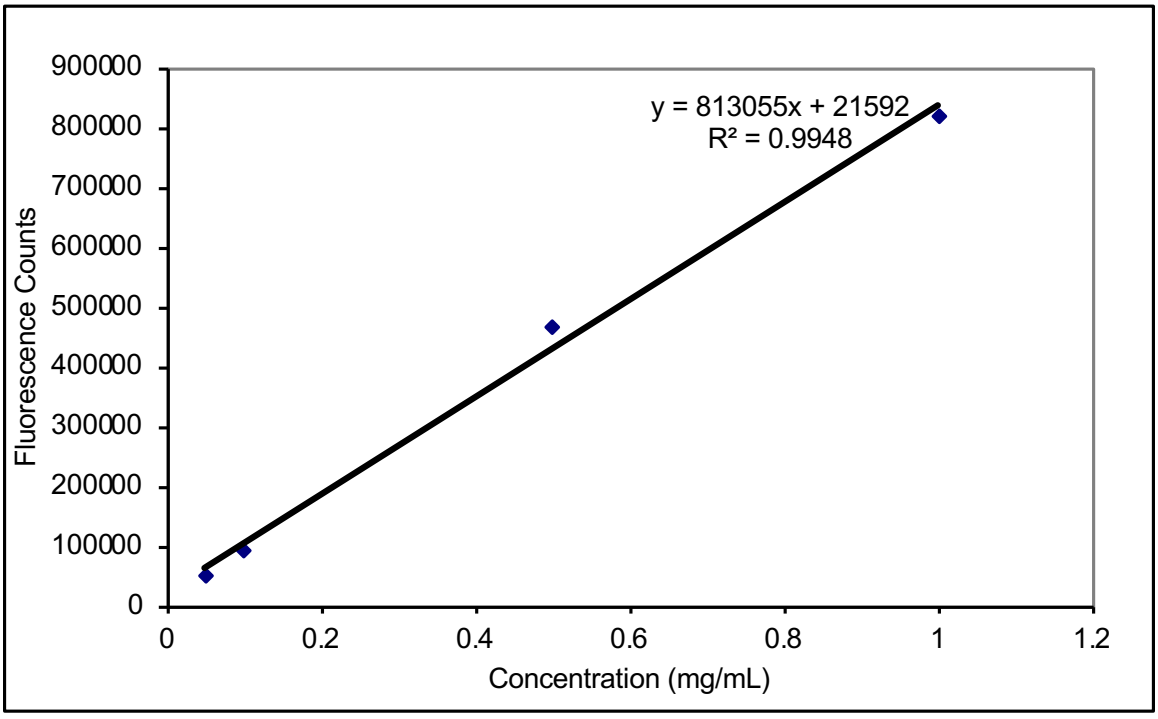

Figure A.0.15. Fluorescence Calibration Curve for **PSGal$_{18}$-Rho**.

JOHN WILEY AND SONS LICENSE TERMS AND CONDITIONS

Apr 30, 2018

This Agreement between Joshua Jadischke ("You") and John Wiley and Sons ("John Wiley and Sons") consists of your license details and the terms and conditions provided by John Wiley and Sons and Copyright Clearance Center.

License Number	4338621402321
License date	Apr 30, 2018
Licensed Content Publisher	John Wiley and Sons
Licensed Content Publication	Angewandte Chemie International Edition
Licensed Content Title	Polyvalent Interactions in Biological Systems: Implications for Design and Use of Multivalent Ligands and Inhibitors
Licensed Content Author	Mathai Mammen, Seok-Ki Choi, George M. Whitesides
Licensed Content Date	Dec 17, 1998
Licensed Content Volume	37
Licensed Content Issue	20
Licensed Content Pages	41
Type of use	Dissertation/Thesis
Requestor type	University/Academic
Format	Print and electronic
Portion	Figure/table
Number of figures/tables	1
Original Wiley figure/table number(s)	Figure 17
Will you be translating?	No
Title of your thesis / dissertation	Glycopolymer Functionalization of Polymersomes
Expected completion date	May 2018
Expected size (number of pages)	90
Requestor Location	Joshua Jadischke 1151 Richmond St. London, ON N6A3K7 Canada Attn: Joshua Jadischke
Publisher Tax ID	EU826007151
Total	0.00 CAD
Terms and Conditions	

Figure A.0.16. Rights and Permission to reprint Figure 1.4.

Curriculum Vitae

Josh Jadischke

Education

M.Sc. Synthetic Organic Chemistry — May 2016 – April 2018
University of Western Ontario, London, ON, Canada
Thesis: *Glycopolymer Functionalization of Polymersomes*

B.Sc. Chemistry — April 2016
University of Western Ontario, London, ON, Canada
Thesis: *Self-healing Phosphonium Polymer Networks*

Awards

Highly Commended Entrant — Nov. 2016

- Award included invitation to present at a conference in Ireland, along with recognition by '*The Undergraduate Awards'*.

Summer Company Grant — Summer 2015

- A grant and training program offered by the Ontario government to support new and high growth potential small businesses.

Scholarship of Excellence — Sept. 2012

- Entrance scholarship based on application average – granted by the University of Western Ontario.

Teaching Experience

TA, Organic Chemistry III, Chemistry Department, 70 h — Fall 2017

TA, Organic Chemistry for Life Sciences, — Fall 2017

Chemistry Department, 140 h

TA, Organic Chemistry of Biological Sciences, Chemistry Department, 140 h — Winter 2017

TA, Organic Chemistry for Life Sciences, Chemistry Department, 70 h — Fall 2016

TA, Organic Chemistry I, Chemistry Department, 70 h — Fall 2016

Publications

Cuthbert, T. J.; **Jadischke, J. J.**; De Bruyn, J. R.; Ragogna, P. J.; Gillies, E. R. Self-Healing Polyphosphonium Ionic Networks. *Macromolecules* **2017**, *50*, 5253–5260.

Presentations

3. **Jadischke, J. J.,** Raycraft, B.R., Whitton, G., Trant, J.F., and Gillies, E.R. Glycopolymer Functionalization of Nanocarriers for Improved Microbial Binding. Poster presentation delivered at Nano Ontario 2017, Toronto, ON, Nov. 2017.

2. **Jadischke, J. J.,** Raycraft, B.R., Whitton, G., Trant, J.F., and Gillies, E.R. Glycopolymer Functionalization of Nanocarriers for Improved Microbial Binding. Poster presentation delivered at Canadian Society for Chemistry Conference and Exhibition, Toronto, ON, May 2017.

1. **Jadischke, J. J.,** Raycraft, B.R., Whitton, G., Trant, J.F., and Gillies, E.R. Glycopolymer-functionalized vesicles via aqueous RAFT polymerization from vesicle surface. Poster presentation delivered at the Fallona Family Interdisciplinary Research Showcase, London, ON, January 2017.